RESEARCH ARTICLE

Fungal Inositol Pyrophosphate IP_7 Is Crucial for Metabolic Adaptation to the Host Environment and Pathogenicity

Sophie Lev,[a] Cecilia Li,[a] Desmarini Desmarini,[a] Adolfo Saiardi,[b] Nicole L. Fewings,[c] Stephen D. Schibeci,[c] Raghwa Sharma,[d] Tania C. Sorrell,[a,e] Julianne T. Djordjevic[a]

Centre for Infectious Diseases and Microbiology, Westmead Millennium Institute, Westmead, and Sydney Medical School-Westmead, University of Sydney, New South Wales, Australia[a]; Medical Research Council Laboratory for Molecular Cell Biology, University College London, London, United Kingdom[b]; Centre for Immunology and Allergy Research, Westmead Millennium Institute, Westmead, New South Wales, Australia[c]; Anatomical Pathology, Westmead Hospital, Westmead, and Universities of Sydney and Western Sydney, New South Wales, Australia[d]; Marie Bashir Institute for Infectious Diseases and Biosecurity, University of Sydney, New South Wales, Australia[e]

ABSTRACT **Inositol pyrophosphates (PP-IPs) comprising inositol, phosphate, and pyrophosphate (PP) are essential for multiple functions in eukaryotes. Their role in fungal pathogens has never been addressed. *Cryptococcus neoformans* is a model pathogenic fungus causing life-threatening meningoencephalitis. We investigate the cryptococcal kinases responsible for the production of PP-IPs (IP_7/IP_8) and the hierarchy of PP-IP importance in pathogenicity. Using gene deletion and inositol polyphosphate profiling, we identified Kcs1 as the major IP_6 kinase (producing IP_7) and Asp1 as an IP_7 kinase (producing IP_8). We show that Kcs1-derived IP_7 is the most crucial PP-IP for cryptococcal drug susceptibility and the production of virulence determinants. In particular, Kcs1 kinase activity is essential for cryptococcal infection of mouse lungs, as reduced fungal burdens were observed in the absence of Kcs1 or when Kcs1 was catalytically inactive. Transcriptome and carbon source utilization analysis suggested that compromised growth of the *KCS1* deletion strain (Δ*kcs1* mutant) in the low-glucose environment of the host lung is due to its inability to utilize alternative carbon sources. Despite this metabolic defect, the Δ*kcs1* mutant established persistent, low-level asymptomatic pulmonary infection but failed to elicit a strong immune response *in vivo* and *in vitro* and was not readily phagocytosed by primary or immortalized monocytes. Reduced recognition of the Δ*kcs1* cells by monocytes correlated with reduced exposure of mannoproteins on the Δ*kcs1* mutant cell surface. We conclude that IP_7 is essential for fungal metabolic adaptation to the host environment, immune recognition, and pathogenicity.**

IMPORTANCE ***Cryptococcus neoformans* is responsible for 1 million cases of AIDS-associated meningitis and ~600,000 deaths annually. Understanding cellular pathways responsible for pathogenicity might have an impact on new drug development. We characterized the inositol polyphosphate kinases Kcs1 and Asp1, which are predicted to catalyze the production of inositol pyrophosphates containing one or two diphosphate moieties (PP-IPs). Using gene deletion analysis and inositol polyphosphate profiling, we confirmed that Kcs1 and Asp1 are major IP_6 and IP_7 kinases, respectively. Kcs1-derived IP_7, but not Asp1-derived IP_8, is crucial for pathogenicity. Global expression profiling and carbon source utilization testing suggest that IP_7-deficient cryptococci cannot adapt their metabolism to allow growth in the glucose-poor environment of the host lung, and consequently, fungal burdens are significantly reduced. Persistent asymptomatic Δ*kcs1* mutant infection correlated with decreased mannoprotein exposure on the Δ*kcs1* mutant surface and reduced phagocytosis. We conclude that IP_7 is crucial for the metabolic adaptation of *C. neoformans* to the host environment and for pathogenicity.**

Received 14 April 2015 **Accepted** 4 May 2015 **Published** 2 June 2015

Citation Lev S, Li C, Desmarini D, Saiardi A, Fewings NL, Schibeci SD, Sharma R, Sorrell TC, Djordjevic JT. 2015. Fungal inositol pyrophosphate IP_7 is crucial for metabolic adaptation to the host environment and pathogenicity. mBio 6(3):e00531-15. doi:10.1128/mBio.00531-15.

Editor Françoise Dromer, Institut Pasteur

Address correspondence to Julianne T. Djordjevic, julianne.djordjevic@sydney.edu.au.

Cryptococcus neoformans var. *grubii* is a basidiomycetous opportunistic human fungal pathogen of global significance that commonly infects immunocompromised hosts, including those with AIDS. *Cryptococcus neoformans* is responsible for ~1 million cases of HIV-associated cryptococcal meningitis and ~600,000 deaths per year worldwide, predominantly in sub-Saharan Africa (1). Cryptococcal lung infection within an immunocompromised host can result from the inhalation of infectious propagules or the reactivation of a latent infection (2). Dissemination from the lungs to the central nervous system (CNS) occurs via the blood or lymphatic system (2). Survival of *Cryptococcus neoformans* within the adverse environment of the host depends on the coordinated functions of multiple stress-related signaling pathways that regulate the expression of a suite of virulence traits and remodeling of the fungal cell wall (3).

Cryptococcal virulence determinants include the ability to grow at host physiological temperature (37°C) and the production of melanin and polysaccharide capsule (for a review, see references 4 to 7). Melanin protects cells from damage caused by reactive oxygen species, which macrophages produce as part of their antimicrobial defense (8). It is deposited in the cell wall via the catalytic activity of the cell wall-associated enzyme laccase (9). The

capsule surrounds the cell wall and is comprised of glucuronoxylomannan (GXM) (90%), galactoxylomannan (GalXM), and highly mannosylated and immunogenic mannoproteins (1%) (10, 11). It protects cryptococci within the host by having a suppressive effect on the host proinflammatory response, by inhibiting the antigen-presenting capability of monocytes, and by rendering cryptococcal cells resistant to phagocytosis by shielding cell wall glucans and mannoproteins from recognition by macrophages and dendritic cells (7, 12, 13). Many mannoproteins are tethered to the cell wall by a glycosylphosphatidylinositol (GPI) anchor (14) and are localized predominantly in the innermost layer of the capsule. However, they can become detached from the anchor and secreted through the capsular layer (15–19). Several of these mannoproteins are potential vaccine candidates against cryptococcal infection (14, 20–22).

The cryptococcal enzyme phospholipase C1 (Plc1) is a component of a stress-related signaling pathway governing the production of a suite of virulence traits, which are compromised when the Plc1-encoding gene is deleted (23). We demonstrated that recombinant Plc1 hydrolyzes the membrane lipid, phosphatidylinositol-bisphosphate (PIP_2) to produce inositol 1,4,5-trisphosphate (IP_3) (23) and that IP_3 is a substrate for cryptococcal Arg1, an inositol polyphosphate kinase (IPK) (24). As with the Δ*plc1* mutant, multiple cryptococcal virulence traits were compromised in the Δ*arg1* mutant (24), suggesting that the absence of more complex inositol polyphosphates (IPs) and/or inositol pyrophosphates (PP-IPs) downstream of Arg1 contributes to the reduced virulence observed for both mutants.

PP-IPs, of which IP_7 and IP_8 are the most physiologically relevant, differ from IPs in that they possess a diphosphate on one or more carbons of the inositol ring. They regulate diverse cellular functions in eukaryotes (25–32). In the nonpathogenic yeasts *Saccharomyces cerevisiae* and *Schizosaccharomyces pombe*, different IP_7 isoforms are essential for growth, vacuole biogenesis, salt tolerance, endocytic trafficking, the function of the cortical actin cytoskeleton, surface adhesion, and dimorphic switching in *S. pombe* (26, 33–37). PP-IPs affect cellular function at both the transcriptional and the posttranslational level via mechanisms that remain to be fully understood. These molecules modulate protein function directly through binding or indirectly by phosphorylating prephosphorylated proteins via a nonenzymatic reaction (38, 39). IP_7 isoforms can also compete with membrane $PI(3,4,5)P_3$ for binding to pleckstrin homology domain-containing proteins, affecting the association of these proteins with the plasma membrane, as observed in *Dictyostelium discoideum* (25). Recently, Worley et al. (40) showed that PP-IPs act in parallel with the TORC1 pathway to control the activity of the class I histone deacetylase Rpd3L and elicit global transcriptional changes in response to different types of stress (40). PP-IPs are therefore central regulators of eukaryotic cellular function, and targeting their synthesis holds promise for the development of new antifungal therapies. However, the kinases directly responsible for the synthesis of PP-IPs in fungal pathogens have not been determined, and the direct role of PP-IPs in regulating fungal pathogenicity remains unclear.

In the present study, we identified two PP-IP-producing kinases, Kcs1 and Asp1 (homolog of *S. cerevisiae* Vip1) in *C. neoformans*, characterized their enzymatic activities, and investigated the role of their products in pathogenicity and cellular function. Since IP_7 was found to be the most crucial PP-IP for cryptococcal pathogenicity, we further investigated its role in cellular function using gene expression and carbon source utilization studies.

RESULTS

Kcs1 is an IP_6 kinase in *C. neoformans*. We identified a putative IP_6 kinase-encoding gene (CNAG_02897/*KCS1*) in *C. neoformans* var. *grubii* (strain H99) using Kcs1 from *S. cerevisiae* in a homology search. The protein encoded by *KCS1* is predicted to be 1,249 amino acids long and to contain an IPK domain at the C terminus. *C. neoformans* Kcs1 (*Cn*Kcs1) has 53% similarity to *S. cerevisiae* Kcs1 (*Sc*Kcs1) at the amino acid level. While the long N-terminal sequences are highly varied among fungal Kcs1 homologs, the C-terminal IPK domains are more conserved: the *Cn*Kcs1 and *Sc*Kcs1 IPK domains share 50% similarity. Phylogenetic analysis of the fungal Kcs1 homologs using full Kcs1 sequences or IPK domains demonstrates that *Cn*Kcs1 is clustered with other Kcs1 homologs of Basidiomycetes (Fig. 1A).

Next, we assessed the role of Kcs1 in cryptococcal IP metabolism by creating a *KCS1* deletion strain (Δ*kcs1* mutant) and comparing its IP profile with that of the wild type (WT) and Δ*arg1* mutant (see Text S1 and Fig. S1A and B in the supplemental material; Fig. 1B). Intracellular IPs in the WT and mutant strains were radiolabeled by adding [^{3}H]myo-inositol to the culture medium, extracted from the cells and fractionated using anion-exchange high-performance liquid chromatography (HPLC). As in *S. cerevisiae* and mammalian cells, the most abundant IP species in the WT was IP_6. Accumulation of IP_3 in the *C. neoformans* Δarg1 mutant was consistent with the findings of our previous study, where raised levels of IP_3 were detected using a radiometric IP_3 binding assay (24). The Δ*arg1* mutant was also deficient in more highly phosphorylated IP species, including the predicted products of Arg1 (IP_4 and IP_5) and IP_6 to IP_8 (IP_{6-8}). In the *C. neoformans* Δkcs1 mutant, the amount of IP_{3-6} was similar to that in the WT. However, the more highly phosphorylated PP-IP_5 (IP_7) and PP_2-IP_4 (IP_8) were not detected, consistent with Kcs1 functioning as the major IP_6 kinase in *C. neoformans*. These results also establish that Arg1 and Kcs1 are components of the same metabolic pathway.

The mammalian IP_6 kinase IP6K1 has been reported to perform physiological functions that are independent of its IP_6 kinase activity (41). Furthermore, *Cn*Kcs1 and *Sc*Kcs1 contain an extended N terminus, which may have additional physiological functions. To distinguish IP_6 kinase-dependent and -independent effects, we created the Δ*kcs1*::*KCS1*^{AAA} strain, in which the sequence encoding conserved amino acids in the Kcs1 catalytic domain (^{1032} SLL^{1034}) was altered to encode AAA, resulting in the expression of kinase-inactive Kcs1 (Text S1; Fig. S1A. This same substitution abrogated Kcs1 catalytic activity in *S. cerevisiae* (34). The Δ*kcs1*::*KCS1*^{AAA} strain was created by ectopic insertion of the mutagenized *KCS1* gene with its native promoter and terminator into the genome of the Δ*kcs1* mutant. A control strain (the Δ*kcs1*::*KCS1* strain) was similarly created by inserting the native *KCS1* genomic fragment ectopically into the genome of the Δ*kcs1* mutant. Integration of *KCS1*^{AAA} and *KCS1* into a single genomic location in each strain was confirmed by Southern blotting (Fig. S1C). The levels of expression of ectopically integrated *KCS1* and *KCS1*^{AAA} in the respective reconstituted strains were comparable to the expression of native *KCS1* in the WT (Fig. S1D). Like the Δ*kcs1* mutant, the Δ*kcs1*::*KCS1*^{AAA} strain did not produce IP_{7-8} (Fig. 1B, inset). The IP profile of the Δ*kcs1*::*KCS1* strain was

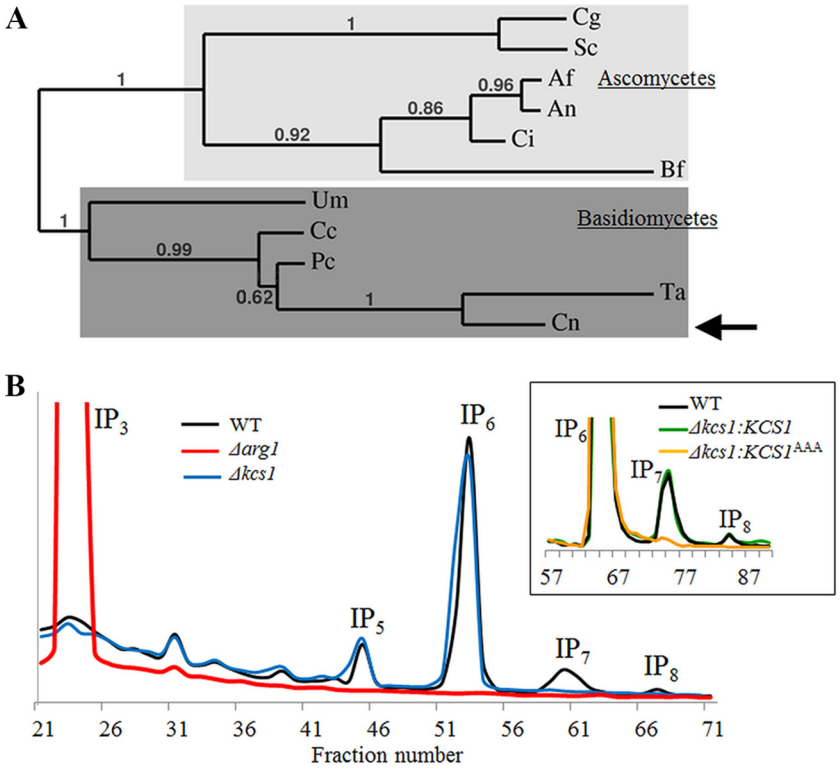

FIG 1 Kcs1 is an IP_6 kinase in *C. neoformans*. (A) Phylogenetic analysis of Kcs1 homologs in fungi. Full-length *C. neoformans* Kcs1 protein (indicated by the arrow) was used to generate the phylogenetic tree. Cg, *Candida glabrata* XP_445605; Sc, *Saccharomyces cerevisiae* Q12494; Af, *Aspergillus fumigatus* XP_753330; An, *Aspergillus nidulans* XP_664484; Ci, *Coccidioides immitis* EAS27460.2; Um, *Ustilago maydis* XP_757030.1; Cc, *Coprinopsis cinerea* XP_001836888; Pc, *Phanerochaete carnosa* EKM59468; Ta, *Trichosporon asahii* EKD02283; Cn, *Cryptococcus neoformans* AFR93794. Numbers represent bootstrap values. (B) Analysis of the inositol polyphosphate profile of the WT, Δ*kcs1*, and Δ*arg1* strains. The inset represents IP profiles of the reconstituted Δ*kcs1* strains: the Δ*kcs1*::*KCS1* strain (expressing native Kcs1) and the Δ*kcs1*::*KCS1*^{AAA} strain (expressing kinase-inactive Kcs1). Intracellular IPs were labeled with [^{3}H]myo-inositol, extracted, and analyzed by anion-exchange HPLC. The elution time for different IP species was determined using standards. The position of each IP species is indicated.

similar to that of the WT (Fig. 1B, inset). The Δ*kcs1* and Δ*kcs1*::*KCS1*^{AAA} strains were subsequently used to identify phenotypes that were specifically associated with the absence of Kcs1 catalytic activity.

Loss of IP_6 kinase activity leads to growth and cell wall integrity defects. The ability of *C. neoformans* to colonize host tissue is dependent on its ability to grow at mammalian physiological temperatures. Since PP-IP products generated by *Sc*Kcs1 play a role in the response to heat stress, the growth of the WT, Δ*kcs1*, and Δ*kcs1*::*KCS1*^{AAA} strains was assessed at 30°C, 37°C, and 39°C using a drop dilution test. Like that of the Sc*Δkcs1* mutant, the growth of the Δ*kcs1* and Δ*kcs1*::*KCS1*^{AAA} strains at all three temperatures was reduced compared to that of the WT and Δ*kcs1*::*KCS1* strain (Fig. 2).

We also investigated the integrity of the cell wall in the Δ*kcs1* and Δ*kcs1*::*KCS1*^{AAA} mutants and their ability to produce mating filaments. Cell wall integrity was assessed by comparing the extent of growth in the presence of cell wall-perturbing agents. Figure 2 demonstrates that the growth of the Δ*kcs1* and Δ*kcs1*::*KCS1*^{AAA} strains was similarly reduced in the presence of SDS and caffeine, compared with that of the WT and Δ*kcs1*::*KCS1* strains, consistent with a cell wall integrity defect. The Δ*kcs1* and Δ*kcs1*::*KCS1*^{AAA} (mating type α) strains also produced fewer mating filaments fol-

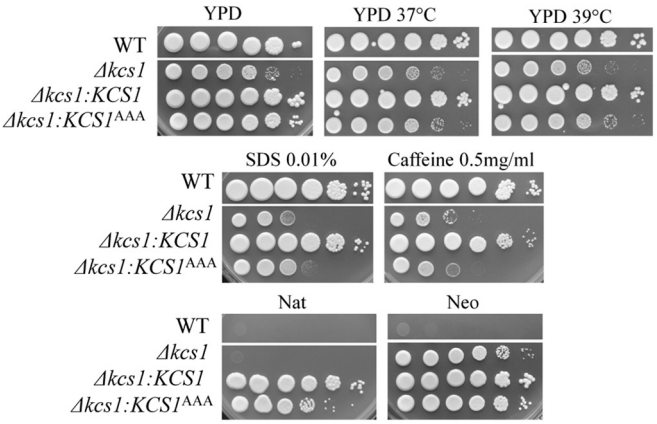

FIG 2 Spot dilution assays demonstrating a cell wall defect in the Δ*kcs1* and kinase-inactive Δ*kcs1*::*KCS1*^{AAA} strains but not in the kinase-active Δ*kcs1*::*KCS1* strain. The strains were serially diluted 10-fold (10^6 to 10 cells/spot from left to right) and spotted onto the test plates indicated. The dual nourseothricin (Nat) and neomycin (Neo) resistance of the Δ*kcs1*::*KCS1* and Δ*kcs1*::*KCS1*^{AAA} strains confirms that integration of the *KCS1* construct (providing Nat resistance) occurred in the Δ*kcs1* mutant strain background (Neo resistance).

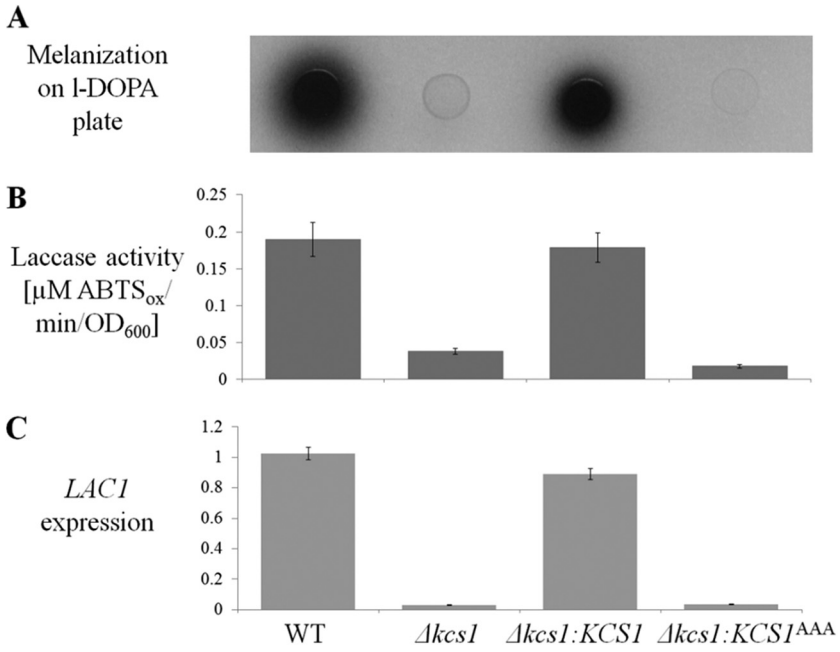

FIG 3 Melanization, extracellular laccase activity, and *LAC1* gene expression are reduced in the Δ*kcs1* and kinase-dead Δ*kcs1*::*KCS1*^{AAA} strains. (A) Cumulative melanization in the WT, Δ*kcs1*, Δ*kcs1*::*KCS1*^{AAA}, and Δ*kcs1*::*KCS1* strains was compared by spotting similar numbers of cells (5 μl; OD_{600} = 3) onto MM plates lacking glucose (laccase inducing) and containing the laccase substrate L-DOPA, and incubating them for 3 days at 30°C. (B) Extracellular laccase activity was quantified spectrophotometrically by measuring the oxidation of the laccase substrate ABTS ($ABTS_{ox}$) by fungal cells following 4 h of growth in MM broth without glucose at 30°C. (C) *LAC1* gene expression was quantified in cultures grown for 5 h in MM broth without glucose by real-time PCR. *ACT1* was used for normalization of expression. The differences between different strains in panels B and C are statistically significant ($P < 0.05$), as determined by Student's *t* test.

lowing a unilateral cross with KN99 (mating type **a**), while filament production was restored to WT levels in the Δ*kcs1*::*KCS1* strain (Fig. S2). Since the cell wall integrity and mating defects persisted in the Δ*kcs1*::*KCS1*^{AAA} strain (Fig. 2; Fig. S2), it can be concluded that the PP-IPs produced by Kcs1 are essential for cell wall integrity and mating.

The Δ*kcs1* mutant is hypersusceptible to antifungal agents. To investigate whether disruption of PP-IP synthesis alters the susceptibility of *C. neoformans* to antifungal drugs, the extent of growth of the WT and the Δ*kcs1* mutant was compared in the presence of amphotericin B, flucytosine, echinocandins, and a range of azoles (Table S1). The Δ*kcs1* mutant was 8 times more susceptible than the WT to posaconazole, voriconazole, itraconazole, and fluconazole and twice as susceptible to flucytosine and amphotericin B but remained resistant to the echinocandins, caspofungin, micafungin, and anidulafungin. The Δ*arg1* mutant demonstrated a similar drug susceptibility profile (Table S1 and Text S1).

The Δ*kcs1* mutant has defective melanin production and an increased capsule size. Next, we assessed the ability of the Kcs1-deficient strains to produce melanin. Melanin protects cryptococci from a variety of stresses, including macrophage-derived oxidative stress and UV light. The Δ*kcs1* and Δ*kcs1*::*KCS1*^{AAA} strains produced less melanin than the WT when grown on minimal medium (MM) without glucose and supplemented with L-3,4-dihydroxyphenylalanine (L-DOPA) (Fig. 3A). The extent of melanization in the Δ*kcs1*::*KCS1* strain was similar to that of the WT. Since the cell wall-associated enzyme laccase 1 catalyzes melanin synthesis in *C. neoformans*, allowing it to be deposited in the cell wall, the extracellular laccase activity associated with intact fungal cells was also measured. The results in Fig. 3B demonstrate that the reduced melanization of the Δ*kcs1* and Δ*kcs1*::*KCS1*^{AAA} strains (Fig. 3A) coincided with reduced extracellular laccase activity as measured by oxidation of the laccase substrate 2,2′-azinobis(3-ethylbenzthiazolinesulfonic acid) (ABTS). Once again, laccase activity was restored to WT levels in the Δ*kcs1*::*KCS1* strain. To determine whether reduced laccase activity in the Kcs1-deficient strains is due to the absence of *LAC1* gene induction under melanin-inducing conditions, we measured *LAC1* expression in the WT, Δ*kcs1*, Δ*kcs1*::*KCS1*, and Δ*kcs1*::*KCS1*^{AAA} strains following 5 h of growth in MM without glucose. Figure 3C demonstrates that the *LAC1* expression profile in all strains is similar to that observed for laccase activity and melanin production. These data indicate that Kcs1-derived PP-IPs are essential for induction of *LAC1*.

Capsule production was also assessed following the growth of fungal strains on Sabouraud (SAB) agar. Notably, colonies formed by the Kcs1-deficient strains had a mucoid (glossy) appearance, in contrast to the dull surface of the WT (Fig. 4A). The capsules produced by the Δ*kcs1* and Δ*kcs1*::*KCS1*^{AAA} strains were on average larger than those produced by the WT (Fig. 4B and C). Colony appearance and capsule size were partially restored in the Δ*kcs1*::*KCS1* strain.

Phenotypic defects in the Δ*kcs1* mutant are caused by the absence of IP_7, not IP_8. Kcs1 is essential for the production of the PP-IPs IP_7 and IP_8, as neither species was detected in the Δ*kcs1* and Δ*kcs1*::*KCS1*^{AAA} strains (Fig. 1B). To determine the relative contribution of IP_8 to the Kcs1-dependent traits, we identified a homolog of the IP_{6-7} kinase of *S. cerevisiae* (*Sc*Vip1) in *C. neoformans*, designated Asp1. Asp1 protein (encoded by CNAG_02161)

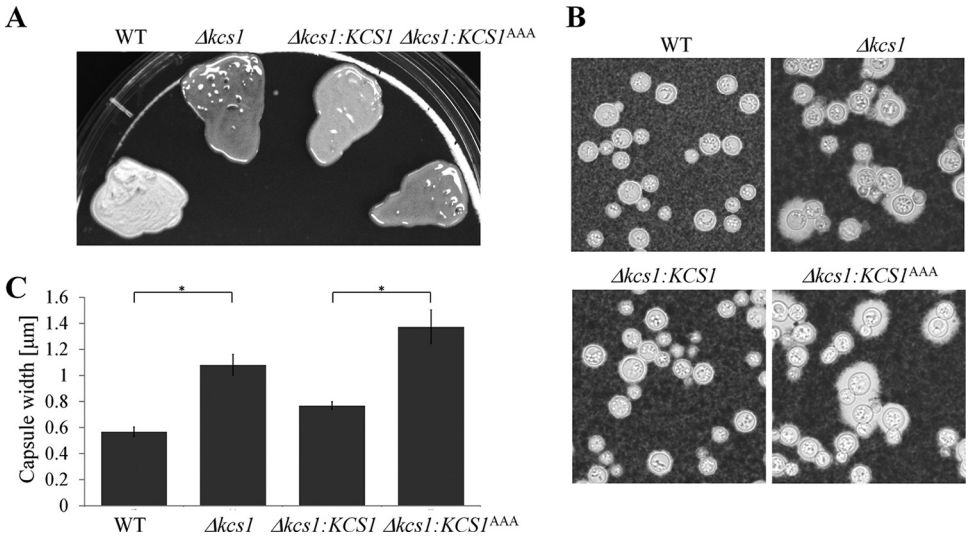

FIG 4 Kcs1 deficiency is associated with a mucoid (glossy) colony appearance (A) and enlarged capsules (B and C). (A) Fungal strains were grown on Sabouraud (SAB) agar plates at ambient temperature for 3 days. (B) The capsules of the SAB agar-grown cells were visualized by negative staining with India ink. (C) Capsule width was measured in at least 30 cells. The increases in capsule sizes observed for the Δ*kcs1* and Δ*kcs1*::*KCS1*^{AAA} strains, relative to the WT and Δ*kcs1*::*KCS1* strains, respectively, are statistically significant (*, $P < 0.05$), as determined using a Tukey-Kramer multiple-comparison test. Error bars indicate standard errors.

is predicted to be 1,117 amino acids long and is 33% identical and 24% similar to *Sc*Vip1. Like *Sc*Vip1 and Asp1 in *Schizosaccharomyces pombe*, Asp1 of *C. neoformans* contains an N-terminal ATP grasp domain responsible for the kinase activity and a C-terminal histidine acid phosphatase domain of unknown function. *C. neoformans ASP1* was deleted as described for *KCS1*, creating the Δ*asp1* mutant. IP_7 accumulated and PP_2-IP_4 (IP_8) was not detected in the Δ*asp1* mutant (Fig. 5), consistent with *C. neoformans* Asp1 functioning as an IP_7 kinase, as reported for *S. cerevisiae* Vip1 (42, 43). A reduction in IP_5 and IP_6 was also noted in the Δ*asp1* strain (Fig. 5). The growth of the Δ*asp1* mutant was assessed under the same conditions as those for the Δ*ksc1* mutant, including 37°C, in the presence of cell wall-perturbing agents, and on mating agar (Fig. S3). The Δ*asp1* strain was also assessed for the production of melanin and capsule. Under all growth conditions, the Δ*asp1* strain exhibited a phenotype similar to that of the WT, indicating that Kcs1-derived PP-IP_5 (IP_7), rather than Asp1-derived PP_2-IP_4 (IP_8), is the most crucial PP-IP for cryptococcal cellular function.

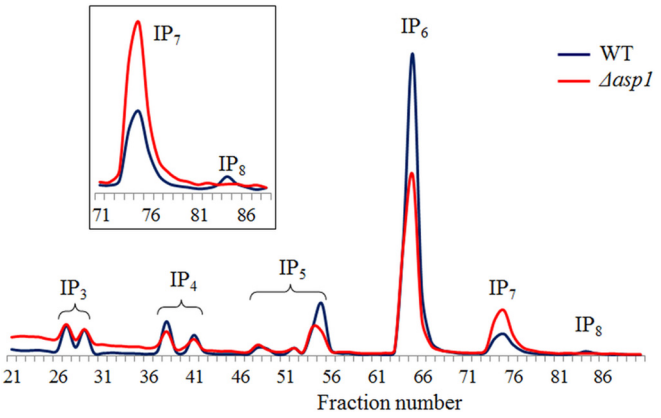

FIG 5 Inositol polyphosphate profile of the Δ*asp1* mutant demonstrating that Asp1 is an IP_7 kinase. The intracellular IPs in the WT and the Δ*asp1* mutant were labeled with [^{3}H]myo-inositol, extracted, and analyzed by anion-exchange HPLC. The elution times for the different IP species indicated were determined using standards. Several IP_3, IP_4, and IP_5 isoforms are discernible in this trace. The inset represents a magnified section of the main graph and demonstrates the accumulation of IP_7 and the reduction of IP_8 in the Δ*asp1* strain.

The Δ*kcs1* mutant is less pathogenic than the WT in animal models. The pathogenicity of the Δ*kcs1* mutant was compared to that of the WT in an invertebrate model, the greater wax moth (*Galleria mellonella*), and a mouse inhalation model. Larvae of *Galleria mellonella* were infected by inoculation of fungi into the lower prolegs and incubated at 30°C. The average survival of Δ*kcs1* mutant-infected larvae was 14 days, compared with 5 days for WT-infected larvae (Fig. 6A). Mice were inoculated via the nares. The median survival time of mice infected with the WT was 14 days. However, no mice succumbed to infection with the Δ*kcs1* mutant for up to 50 days postinoculation (Fig. 6B). Virulence was almost restored by the introduction of *KCS1* into the Δ*kcs1* mutant, with the median survival time of Δ*kcs1*::*KCS1* strain-infected mice being 18 days. Despite the avirulent phenotype, Δ*kcs1* cells were detected in mouse lungs (3×10^3 to 90×10^3 CFU per total lung tissue) over the 50-day postinfection period (Fig. 6C). The Δ*kcs1* mutant infection burden was ~8-fold lower than that of the WT at 3 days postinfection. However, the difference between the WT and the Δ*kcs1* mutant pulmonary burdens increased to ~140-fold at the onset of the inflammatory response 7 days postinfection (see Fig. 7) and to ~286-fold 14 days postinfection. These increases were due primarily to the more rapid increase in WT pulmonary burden than in Δ*kcs1* mutant burden over this time. Despite the persistence of Δ*kcs1* mutant in lungs up to 50 days postinfection, no colonization of the brain was observed during this time (Fig. 6D). This was in contrast to what occurred with mice infected with the WT, which developed a CNS infection by day 14 (the median survival time of WT-infected mice).

Periodic acid-Schiff (PAS)-stained sections of WT- and Δ*kcs1* mutant-infected lungs at day 7 and day 14 are shown in Fig. S4 in

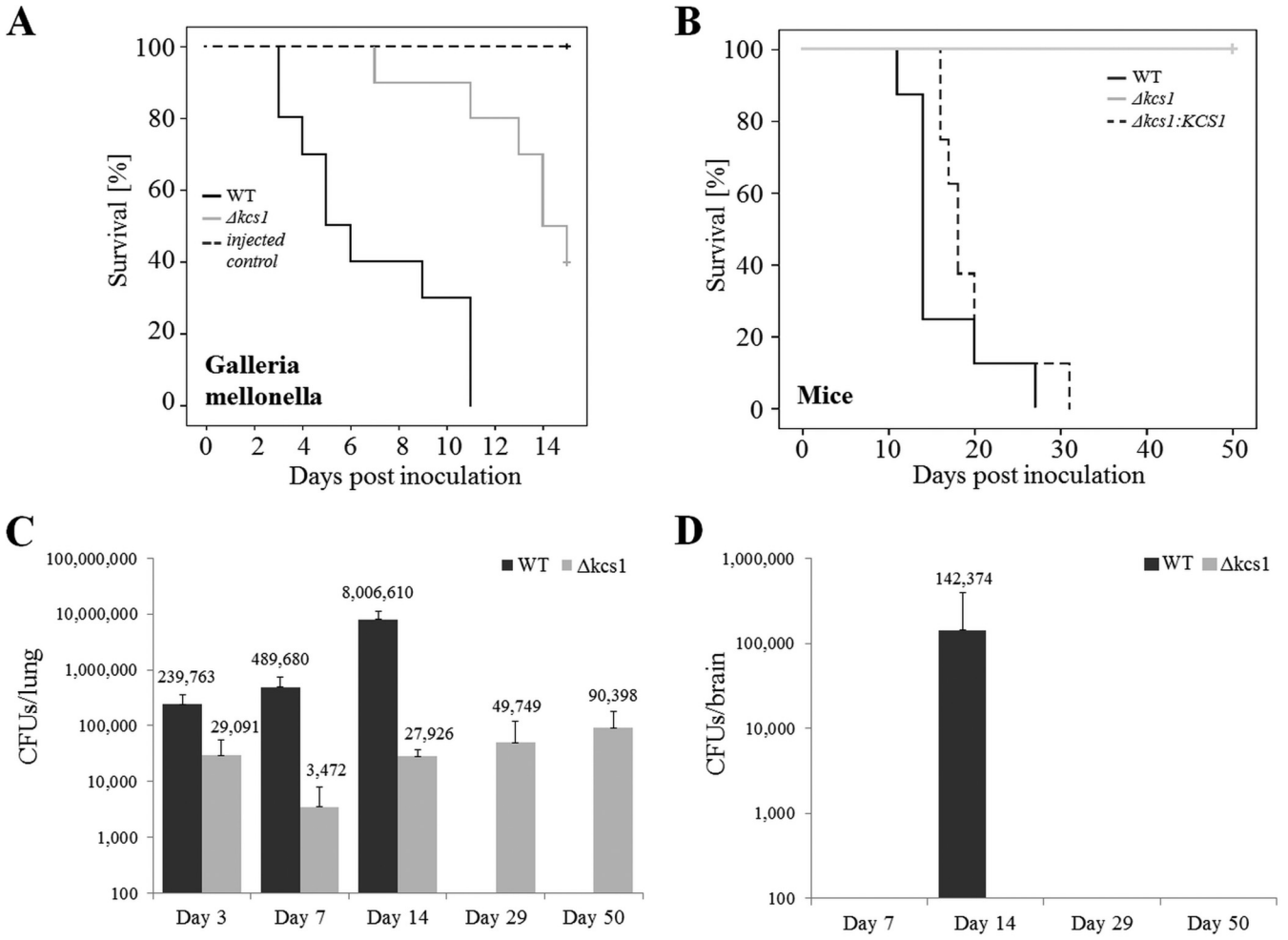

FIG 6 Ksc1 is essential for pathogenicity in *Galleria mellonella* and mice. (A) *G. mellonella* larvae were inoculated with the WT or the Δ*kcs1* mutant (10^6 yeast cells/10 μl). Two groups of larvae were also mock infected with water, or not at all, to serve as controls. The larvae were incubated at 30°C for 10 days, their health was monitored, and their deaths were recorded. (B to D) Anesthetized mice were inoculated intranasally with 5×10^5 CFU/20 μl of the indicated strains and euthanized after exhibiting debilitating symptoms of infection for the survival study (B) or at 3, 7, and 14 days postinfection for organ burden analysis (C and D). (A and B) Δ*kcs1* mutant-infected animals not showing clinical symptoms of illness were culled at days 15 and 50, and censorship of these infection groups is indicated by the cross. The Kaplan-Meier log rank test was used to determine differences in survival, with Δ*kcs1* mutant-infected larvae and mice surviving longer than WT-infected animals and the reconstituted strain in the case of the mouse study (*, $P < 0.05$). The difference in survival of mice infected with the WT and Δ*kcs1*::*KCS1* strain was insignificant ($P = 0.161$). Lungs (C) and brain (D) were removed and homogenized for organ burden analysis (CFU per organ) using quantitative culture.

the supplemental material. A dense WT infection was observed on both days within the alveolar spaces and bronchi, with evidence of extensive infiltration of monocytes and polymorphs. In contrast, but consistent with organ burden analysis, Δ*kcs1* mutant infection was sparse and lung tissue was healthier than in WT-infected lung, as indicated by large areas of well-aerated alveoli and minimal evidence of inflammation. Despite the death of Δ*kcs1* mutant cells over the infection time course, budding cells were observed in the infected lung tissue.

The Δ*asp1* mutant was also tested for virulence in a mouse inhalation model, and the progression of disease in Δ*asp1* mutant-infected animals was found to be similar to that of WT-infected animals. This was expected, as no phenotypic differences were observed between the WT and the Δ*asp1* strain (Fig. S3 and S5).

Δ*kcs1* mutant infection elicits a weak host immune response. The persistent, asymptomatic Δ*kcs1* mutant infection observed in the mouse model (Fig. 6C) prompted us to compare the immune responses elicited by the WT and the Δ*kcs1* mutant. The cytokine profile in infected lung tissue at 3, 7, and 14 days postinoculation was determined by analyzing the supernatants of homogenized lung extracts prepared from WT-, Δ*kcs1* mutant-, and mock-infected animals using a cytokine bead array (CBA) and flow cytometry (Fig. 7).

WT infection elicited a strong proinflammatory response in the lung (gamma interferon [IFN-γ] and tumor necrosis factor [TNF]), which peaked at day 7 postinfection; the day 7 response for IFN-γ and TNF-α was 36- and 3-fold higher than the day 3 response, respectively, and ~688- and 27-fold higher than the response observed in mock-infected animals (Fig. 7). TNF is required for neutrophil recruitment into pulmonary tissue during a cryptococcal infection (44), and IFN-γ maintains monocyte-derived macrophages in an activated state conducive to fungal

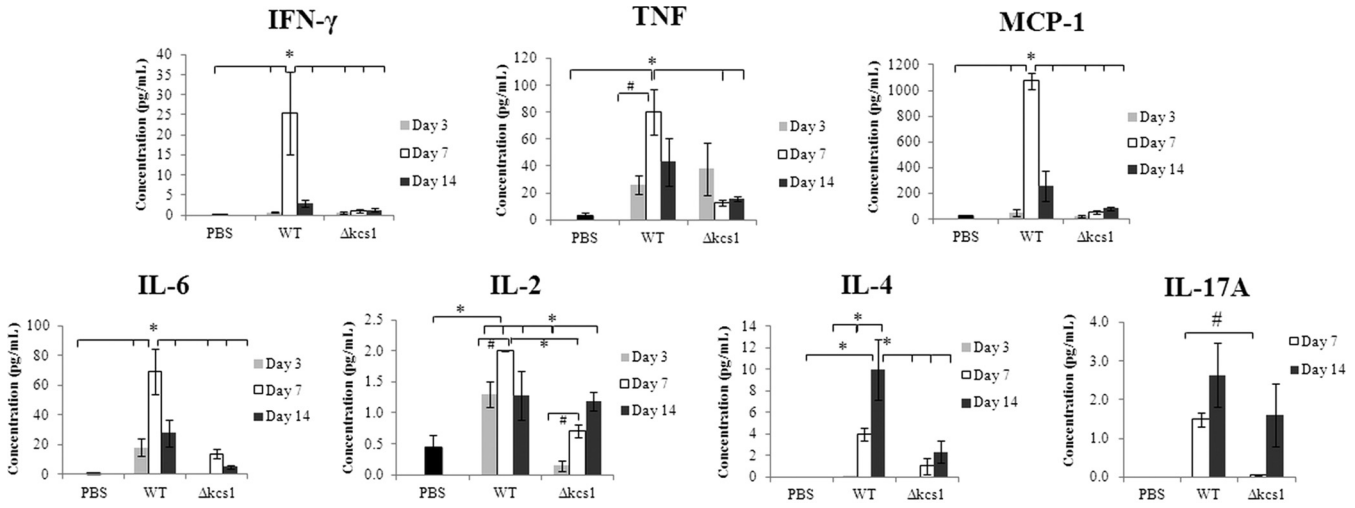

FIG 7 Cytokine profile in mock (PBS)-, WT-, and Δ*kcs1* mutant-infected mouse lung. Lungs of control and *C. neoformans*-infected mice (3 mice/strain/time point) were homogenized, and the concentrations of the indicated cytokines in the supernatant were measured using a cytometric bead array. The IL-10 responses on all days and the IL-17A response at day 3 for both the WT- and the Δ*kcs1* mutant-infected mice were below the level of sensitivity (not shown). *, $P < 0.05$ using a one-way analysis of variance (ANOVA) and a Tukey-Kramer multiple-comparison test; #, $P < 0.05$ using a two-tailed Student *t* test.

killing and clearance. The strong proinflammatory response in WT-infected mice was accompanied by a strong monocyte chemoattractant protein-1 (MCP-1) response, which also peaked at day 7. MCP-1 is a crucial mediator of monocyte and T cell recruitment to the sites of infection. At day 7, the MCP-1 response was 22-fold higher than the day 3 response and 40-fold higher than the response observed in mock-infected animals. Despite the decrease in MCP-1 levels at day 14, significant numbers of monocytes were present at this time point in WT-infected lung (Fig. S4). In contrast to WT, no increase in the level of any of these three cytokines was observed in Δ*kcs1* mutant-infected lung at 7 days, despite evidence of persistent Δ*kcs1* mutant infection. Interleukin 6 (IL-6) production also peaked in WT-infected lung at day 7, with the response being ~4-fold higher than at day 3 and ~84-fold higher than the response observed in mock-infected animals. In contrast to the proinflammatory cytokines and MCP-1, IL-6 production peaked at day 7 in Δ*kcs1* mutant-infected lungs and was ~36-fold higher than the day 3 response and ~17-fold higher than the response observed in mock-infected animals.

IL-2 levels increased in Δ*kcs1* mutant-infected lungs over the time course but particularly from day 3 to day 7. However, the day 3 level was lower than the mock-infected control and WT values, while the day 7 level was similar to that of the mock-infected control but lower than the WT value. Interestingly, similar IL-2 responses were obtained for WT- and Δ*kcs1* mutant-infected lungs at day 14 despite the significantly lower Δ*kcs1* mutant fungal burden. In contrast to that of the other cytokines, IL-4 and IL17-A production was higher at day 14 than at day 7 in WT-infected lungs. However, the IL-4 response observed for Δ*kcs1* mutant-infected lungs did not change significantly between days 7 and 14 but was still higher than the response observed in mock-infected lungs (Fig. 7).

For both the WT and Δ*kcs1* strains, IL-17A levels at day 3 were below the level of detection and are not shown. At day 7, the IL-17A level in Δ*kcs1* mutant-infected lung was lower than that in WT-infected lung, while at day 14, a similar IL-17A response occurred in WT- and Δ*kcs1* mutant-infected lungs, despite the significantly lower Δ*kcs1* mutant burden.

The phagocytosis of the Δ*kcs1* mutant by monocytes and subsequent monocyte activation are compromised. Monocytes and macrophages are the first line of defense against cryptococcal infection. Since we observed an altered surface phenotype in the Kcs1-deficient mutants (Fig. 4A), which may affect cryptococcal recognition by monocytes, we compared the efficiencies of phagocytosis of the WT and Δ*kcs1* mutant *in vitro*, using the THP-1 monocytic cell line. Fungal cells were labeled with fluorescein isothiocyanate (FITC) and opsonized with human serum (containing complement and antifungal antibodies), and their uptake was measured by flow cytometry. Figure 8A demonstrates that after 4 h of coincubation, ~40% of THP-1 cells were associated with WT *C. neoformans*. However, only ~10% of THP-1 cells were associated with Δ*kcs1* cells. Figure S6A shows a representative scatterplot used for quantification of adhesion/uptake. The extent of THP-1 cell association with the WT and Δ*kcs1* mutant was also measured when IgG antibodies purified from human blood were used as the opsonizing agent. The results in Fig. 8A show that only ~20% of THP-1 cells were associated with WT *C. neoformans*, indicating that the combination of complement and antibody is a more potent opsonin of WT cryptococci than antibody alone. As with the results observed for serum opsonization, the number of THP-1 cells associated with IgG-opsonized Δ*kcs1* cells was reduced. Notably, the difference in THP-1 cell association between the WT and mutant was even greater when IgG was used as an opsonin than when serum was used (9-fold versus 4-fold). The extent of THP-1 cell association with the WT and Δ*kcs1* strains was also measured when anticapsular antibodies were used as the opsonizing agent (Fig. 8A). However, in this case, the extents of THP-1 association with the WT and Δ*kcs1* mutant were similar.

To rule out the possibility that Δ*kcs1* cells are taken up less by THP-1 monocytes due to their lower rate of proliferation, we compared the phagocytosis of heat-killed WT and Δ*kcs1* mutant. As with live cryptococci, the phagocytosis of dead Δ*kcs1* cells was

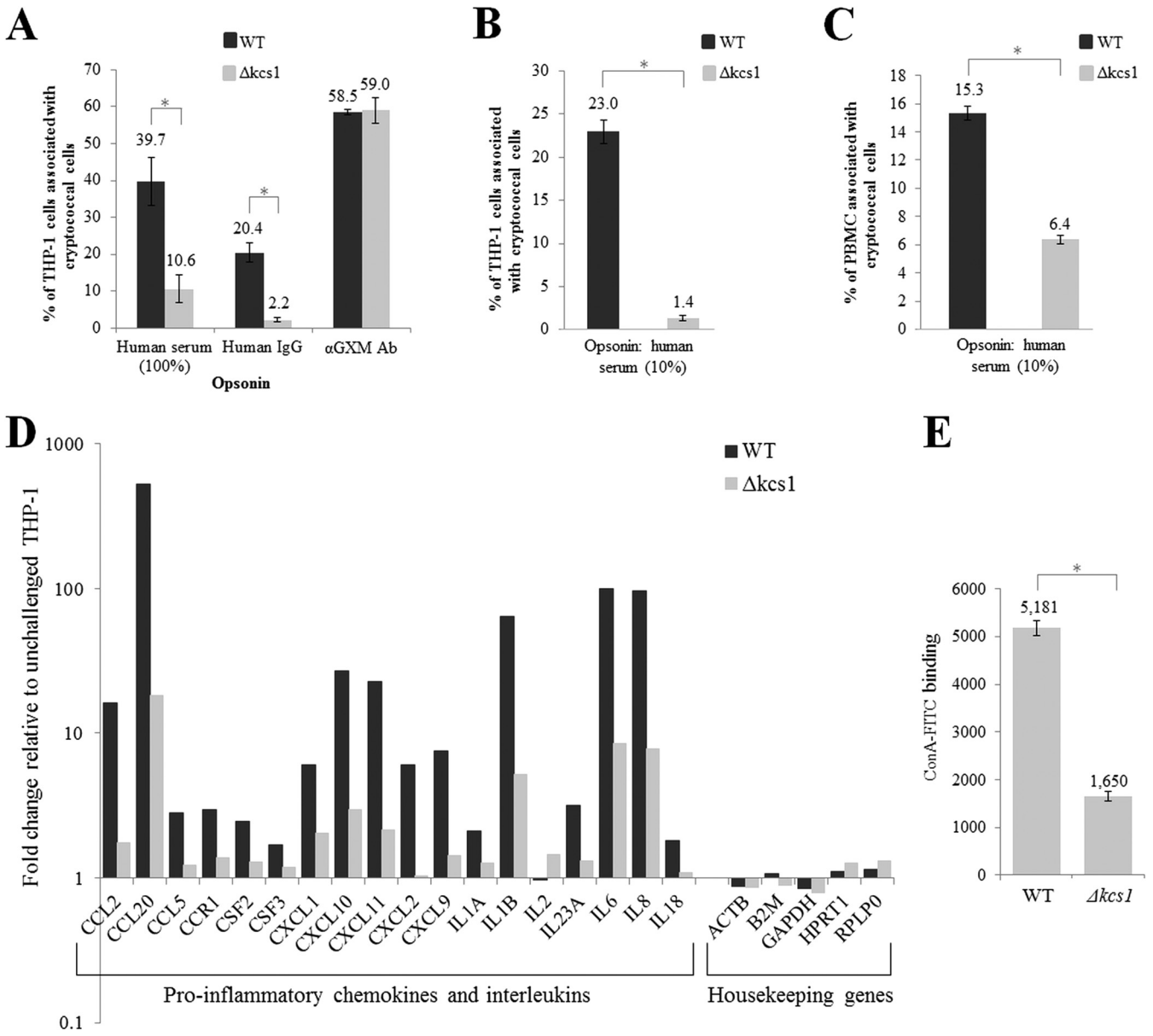

FIG 8 Reduced phagocytosis of Δ*kcs1* cells by monocytes correlates with reduced monocyte activation and reduced binding of concanavalin A. (A) Live FITC-labeled WT and Δ*kcs1* cells were opsonized with 100% serum, purified human IgG, or anti-GXM antibodies and cocultured with activated THP-1 monocytes for 4 h, and the extent of adhesion/uptake was measured by flow cytometry. (B) As in panel A, except that cells were heat killed and opsonized with 10% human serum. (C) As in panel B, except that CD14-positive monocytes within a PBMC preparation were used instead of THP-1 cells. (D) The expression of chemokine- and interleukin-encoding genes in activated THP-1 cells following coculture with serum-opsonized WT and Δ*kcs1* cells was quantified using an RT^2 profiler PCR array designed for analysis of the antifungal response. The expression data were normalized to the expression of the housekeeping genes indicated and then calculated as the fold change from the expression of activated THP-1 cells that had not been coincubated with *C. neoformans*. (E) Each culture was incubated with ConA-FITC and the fluorescence quantified using flow cytometry. The bar graph represents the average fluorescence of WT and Δ*kcs1* cells. Except for those in panel D, all results represent the means and standard deviations of results from biological triplicates. *, $P < 0.005$ using an unpaired, two-tailed *t* test.

reduced (Fig. 8B). The extents of adhesion/uptake of heat-killed cryptococcal cells were also compared in primary human CD14-positive monocytes in a peripheral blood mononuclear cell (PBMC) preparation. Monocytes were distinguished from T and B cells by the binding of fluorescent anti-CD14. As with THP-1 cells (Fig. 8A and B), monocyte uptake of heat-killed, serum-opsonized Δ*kcs1* cells by CD14-positive monocytes was reduced (Fig. 8C). Microscopy of the cocultures also revealed reduced association of the Δ*kcs1* mutant with THP-1 cells and PBMCs (Fig. S6B), consistent with the flow cytometry analysis of fungal adhesion/uptake.

To determine whether reduced phagocytosis of Δ*kcs1* cells by monocytes coincided with reduced monocyte activation, we compared levels of THP-1 activation in the presence of live WT or Δ*kcs1* cells after 4 h of coincubation, using an RT^2 profiler PCR array. The results in Fig. 8D indicate that the expression of proin-

TABLE 1 The expression of genes encoding extracellular proteins is lower in Δ*kcs1* cells than in WT cells

Identifier	Description	Relative expression of[a]: WT cells (fpkm)	Δ*kcs1* cells (fpkm)	WT/Δ*kcs1* (fold change)	Presence of: O-linked glycosylation	N-linked glycosylation	GPI
CNAG_06291	Polysaccharide deacetylase Fpd1 (D25)	410.5	28.88	14.2			
CNAG_03465	Laccase	99.52	9.259	10.7	+	+	
CNAG_06346	Lipoprotein A	180.3	20.23	8.91			
CNAG_02225	Glucan 1,3-β-glucosidase	335.3	53.46	6.27			
CNAG_01758	Polygalacturonase	67.41	12.8	5.27		+	
CNAG_06260	α-Glucosidase	42.12	8.581	4.91			
CNAG_04944	Glycosyl hydrolase family 88	176.5	34.34	5.14			+
CNAG_04735	Elastinolytic metalloproteinase	517.4	111.7	4.63	+	+	
CNAG_06213	Pepsin, aspartic protease	180.8	38.86	4.65	+	+	
CNAG_06501	1,3-β-Glucanosyltransferase	187	46.21	4.05	+	+	+
CNAG_04380	Aspartic peptidase	14.6	3.913	3.73	+		+
CNAG_00488	Phospholipase B1-like lipase	26.23	5.983	4.38	+	+	
CNAG_01040	Carboxypeptidase D	11.72	3.38	3.47		+	
CNAG_07638	PLC-like phosphodiesterase	206.5	70.22	2.94	+	+	+
CNAG_00581	Aspartic peptidase	1652	607.3	2.72	+		
CNAG_06251	Ser/Thr protein phosphatase	5.526	2.085	2.65	+	+	
CNAG_07600	β-Glucosidase	112.5	40.76	2.76	+		
CNAG_04625	Serine-type endopeptidase	339.1	139.7	2.43	+		
CNAG_05471	α-Glucosidase	15.81	6.75	2.34	+	+	
CNAG_05973	Serine carboxypeptidase	15.17	6.594	2.3	+		
CNAG_05411	Endoglucanase	80.12	37.08	2.16	+	+	
CNAG_07865	Ferro-O_2-oxidoreductase	44.08	21.82	2.02	+		

[a] Normalized fpkm values (fragments per kilobase of exon per million reads mapped) were generated by the Galaxy-based Cuffdiff tool and used as a measure of gene expression.

flammatory cytokine- and interleukin-encoding genes is significantly higher in THP-1 cells coincubated with WT than with Δ*kcs1* cells, consistent with the stronger cytokine induction profile observed in the WT-infected mouse lung (Fig. 7). For example, the induction of the gene encoding the monocyte chemoattractant protein (Mcp1/Ccl2) was >9-fold higher in THP-1 cells coincubated with the WT than in cells coincubated with the Δ*kcs1* mutant. Thus, the reduced rate of Δ*kcs1* cell phagocytosis correlated with reduced monocyte activation.

Mannoprotein exposure at the Δ*kcs1* cell surface is reduced. The similar rates of phagocytosis of anti-GXM-opsonized WT and Δ*kcs1* cells suggest that the antibody binds similarly to the surfaces of both strains despite their microscopic (larger capsule size) and macroscopic (mucoid colony morphology) differences. The difference in phagocytosis of WT and Δ*kcs1* cells observed when serum or human IgG were used for opsonization suggests that the respective opsonins bind to surface epitopes other than the sugar moiety binding targets of anti-GXM antibodies. Furthermore, the data suggest that the targets of serum and human IgG opsonins are present in greater amounts on WT than on Δ*kcs1* cells. The capsule contains mannoproteins, in addition to polysaccharides, and human serum contains antibodies against fungal mannoproteins that can initiate classical pathway activation upon binding to macrophages (45). To investigate mannoprotein exposure at the surfaces of WT and Δ*kcs1* cells, the extents of concanavalin A (ConA) binding were compared. ConA is a lectin that reacts with surface mannose sugars found on many microbes and is available as an FITC conjugate so that binding can be assessed by flow cytometry. The results in Fig. 8E show that ConA-FITC binding to the Δ*kcs1* cell surface is decreased in comparison with binding to WT cells, suggesting that mannosylated proteins are not displayed normally on the surface of the mutant cells.

To determine whether the reduced presence of mannoproteins on the Δ*kcs1* cell surface correlates with reduced expression of genes encoding mannoproteins, we performed transcriptome sequencing (RNA-seq) of the WT and Δ*kcs1* strains. We focused on genes encoding proteins with a signal peptide which targets them to the endoplasmic reticulum (ER)/Golgi complex and then to the cell periphery, excluding transmembranal proteins and proteins likely to be mitochondrial, peroxisomal, or ER resident. The expression of 22 extracellular proteins was down-regulated in the mutant, with 17 predicted to be glycosylated and 4 containing a GPI anchor (Table 1). Taken together, the data indicate that Kcs1-derived IP_7 affects the fungal surface composite at the transcriptional level, influencing the extent of opsonization and phagocytosis and the ensuing immune response.

Transcriptome analysis identifies metabolic changes in the Δ*kcs1* mutant. The gene expression profiles of the WT and Δ*kcs1* strains obtained by RNA-seq were further analyzed to identify changes in gene expression that could be responsible for the altered phenotype and virulence profile of the Δ*kcs1* mutant. Initial functional classification of differentially expressed genes was made using gene ontology (GO) term assignment generated by the Joint Genome Institute (JGI) and then refined further based on published literature and by performing a homology search. We found that the absence of IP_7 resulted in an 11-fold reduction in the expression of the *LAC1* gene involved in melanization, consistent with the results in Fig. 3. However, the most significant changes were observed in metabolic function. Tables 2 and S3 demonstrate that genes encoding proteins involved in glycolysis are more highly expressed in the Δ*kcs1* mutant than in the WT. Genes involved in mRNA translation and ribosomal biosynthesis are also more highly expressed in the Δ*kcs1* mutant. However, expression of genes encoding numerous sugar transporters and

TABLE 2 Summary of the RNA-seq data analysis

Functional group	No. of genes upregulated in the Δ*kcs1* mutant	No. of genes downregulated in the Δ*kcs1* mutant	Total no. of genes in the functional group	Significance of enrichment (*P* value)
Glycolysis and pyruvate decarboxylation	4		6	0.0055
Translation/ribosomal biogenesis	91		160	5.32e–37
Citric acid cycle		5	16	0.0273
Fatty acid β-oxidation and peroxisomal organization		18	24	4.58e–13
Glyoxylate cycle and gluconeogenesis		3	5	0.0120
Sugar transporters		23	51	9.06e–10
GO term-assigned genes	545	417	3689	

enzymes that comprise metabolic pathways involved in the utilization of alternative carbon sources (citric acid and glyoxylate cycles, gluconeogenesis, and fatty acid β-oxidation) is reduced in the Δ*kcs1* mutant. These metabolic differences suggest that WT, but not Δ*kcs1*, cells actively express genes involved in the utilization of carbon sources other than glucose, including lactate and fatty acids, which require mitochondrial function.

The environment of the host lung is low in glucose (46), and enzymes involved in the use of alternative carbon sources are essential for cryptococcal pathogenicity (47–49). We therefore compared the extent of growth of both strains on glucose and three nonfermentable carbon sources, lactate, glycerol, and oleic acid, each present as the sole carbon source. We also used minimal medium (MM), which is more physiological than yeast extract-peptone-dextrose (YPD) (Fig. 2) . In MM supplemented with glucose Δ*kcs1* mutant grew similar to the WT strain (Fig. 9A). Glycerol is incorporated into the glycolytic/gluconeogenesis pathway following conversion to dihydroacetone phosphate by mitochondrial flavin adenine dinucleotide (FAD)-dependent glycerol-3-phosphate dehydrogenase. Lactate is converted to pyruvate, which is channeled into the citric acid cycle and gluconeogenesis. Oleic acid undergoes β-oxidation in mitochondria and/or peroxisomes to generate acetyl coenzyme A (acetyl-CoA), which can be used for energy generation via the citric acid cycle. The results in Fig. 9A demonstrate that in contrast to that on glucose, the growth of Δ*kcs1* cells on the alternative carbon sources was severely compromised.

Using quantitative PCR (qPCR) and minimal medium containing glucose or lactate, we compared the levels of expression of a gene encoding a key enzyme in gluconeogenesis, phosphoenolpyruvate carboxykinase (*PCK1*; CNAG_04217) (Fig. 9B). Pck1 catalyzes an irreversible step of gluconeogenesis, and its expression was 20-fold lower in Δ*kcs1* cells grown overnight in YPD than in WT cells under the same conditions (Table S3). In minimal medium supplemented with glucose, *PCK1* expression was 4.5-fold lower in Δ*kcs1* than in WT cells (Fig. 9B), consistent with the global expression data. In the absence of glucose (minimal medium with lactate), *PCK1* was induced in both strains, but its expression was 2-fold lower in the Δ*kcs1* mutant, indicating that gluconeogenesis is not fully activated in the absence of IP_7. This result confirms that the mutant is compromised in its ability to metabolize alternative carbon sources and that the defect is caused, at least in part, by inadequate transcriptional regulation of metabolic enzymes.

DISCUSSION

Delineation of the IP biosynthesis pathway in *C. neoformans*. Using gene deletion analysis and HPLC-based radiometric IP profiling, we have confirmed that Arg1 is an IP_3 kinase. Furthermore, we have demonstrated that the role of Arg1 is to provide IP precursors for the PP-IP-producing kinase Kcs1, which, like Arg1, is essential for cryptococcal virulence. We determined that Kcs1 is the major IP_6 kinase in *C. neoformans*, since it is essential for the synthesis of PP-IP_5 (IP_7) and PP_2-IP_4 (IP_8). In particular, neither the Δ*kcs1* mutant nor the kinase-inactive mutant produced de-

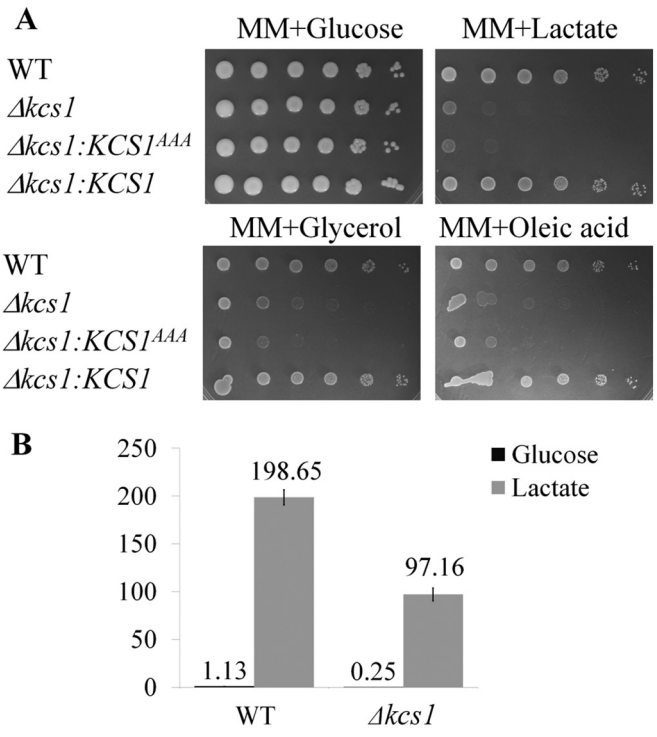

FIG 9 The Δ*kcs1* mutant is defective in its ability to utilize nonfermentable carbon sources. (A) Drop dilution assay. The strains were serially diluted 10-fold (10^6 to 10 cells/spot from left to right) and spotted onto the test plates as indicated. (B) To compare the levels of expression of phosphoenolpyruvate carboxykinase *PCK1* in WT and Δ*kcs1* cells, the strains were grown on YPD, washed, and incubated in MM plus 1% glucose or MM plus 1% sodium lactate broth for 4 h. *PCK1* expression was quantified by qPCR using the housekeeping gene *ACT1* for normalization. The differences between WT and Δ*kcs1* cells grown in the same medium are statistically significant ($P < 0.05$), as determined by Student's *t* test. Error bars indicate standard deviations.

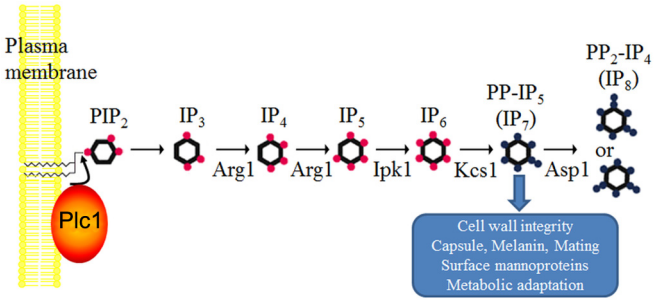

FIG 10 Schematic representation of the inositol polyphosphate biosynthesis pathway in *C. neoformans*. Phospholipase C1 (Plc1) hydrolyzes PIP_2 to produce IP_3. Arg1 is a dual-specificity kinase converting IP_3 to IP_4 and IP_4 to IP_5. Ipk1 is the proposed IP_5 kinase, providing IP_6 as a substrate for Kcs1. Kcs1 is the major IP_6 kinase generating PP-IP_5 (IP_7), and Asp1 is an IP_7 kinase generating PP_2-IP_4 (IP_8). The physiological roles of Kcs1-derived IP_7 are indicated.

tectable amounts of IP_7 (or IP_8). We also showed that Asp1 functions primarily as an IP_7 kinase, converting Kcs1-generated IP_7 to IP_8. In *S. cerevisiae*, IP_7 is also produced by an Asp1 homolog, Vip1 (42). However, our IP profiling revealed that Asp1 does not contribute significantly to IP_7 production in *C. neoformans*. Based on the IP profile obtained for the Δ*arg1*, Δ*kcs1*, and Δ*asp1* mutants, we propose a model of the IP biosynthesis pathway in *C. neoformans* depicted in Fig. 10. The presence of a putative IP_5 kinase (Ipk1) in the middle of the pathway can be inferred from its homology to Ipk1 in *S. cerevisiae*; its role in *C. neoformans* is currently being investigated in our laboratory.

The IP biosynthetic pathway as a drug target. Two observations support investigation of the fungal PP-IP biosynthetic pathway as a potential antifungal drug target: (i) the absence of redundancy in the fungal pathway compared with the mammalian pathway and (ii) low sequence similarity between fungal and mammalian enzymes. For example, while Arg1 in *C. neoformans* is the only enzyme able to convert IP_3 to IP_4, three IP_3 kinase isoforms and the inositol polyphosphate multikinase (IPMK) catalyze this reaction in humans. Arg1 differs structurally and functionally from mammalian IP_3 kinases, implying potential selectivity of inhibition (50, 51). Arg1 and IPMK are only 19% identical, while Kcs1 is even less similar (13% identity) to its mammalian equivalent, inositol hexakisphosphate kinase 1 isoform 1. The hypersusceptibility of Δ*arg1* and Δ*kcs1* cells to antifungal agents (Table S1) also suggests that inhibitors of fungal Kcs1 or Arg1 may act synergistically with these marketed antifungal drugs to provide a better treatment outcome.

Kcs1-derived IP_7, but not Asp1-derived IP_8, is required for optimal growth and the production of virulence traits. We observed delayed growth of the *Cn*Δ*kcs1* mutant under standard growth conditions and a cell wall integrity defect but no high-temperature growth defect. In a cross with the KN99 MAT**a** strain, the Δ*kcs1* mutant, but not the Δ*asp1* mutant, produced stunted mating filaments. Defective Δ*kcs1* cell walls may affect retention of the sexual agglutinins and adhesins, which are required for efficient cell contact prior to filamentation (52), as well as capsule attachment. A mucoid phenotype, typical of the Δ*kcs1* mutant, is likely to be associated with increased capsule size. Such a correlation was also observed in *C. neoformans* following phenotypic switching (53) and in the allergen 1 (*ALL1*) deletion mutant (54). During glucose deprivation, the Δ*kcs1* strain, but not the Δ*asp1* strain, fails to produce extracellular laccase and, consequently, melanin. We established that Kcs1-derived IP_7 affects melanization at the transcriptional level, as the gene encoding the major melanin-producing enzyme in *C. neoformans*, laccase 1 (*LAC1*), was not induced in Δ*kcs1* cells. Transcriptional profiling data supported this finding.

IP_7-dependent metabolic adaptation affects growth and pathogenicity. The inability of the Δ*kcs1* mutant to achieve high infection burdens in mouse lung is most likely multifactorial, due to its weakened cell walls, inability to produce melanin, and reduced growth rate. High-throughput analysis of gene expression in the WT and Δ*kcs1* mutant suggested that the Δ*kcs1* mutant has a reduced ability to utilize carbon sources other than glucose and that this metabolic dysfunction may be a potential reason for its reduced ability to colonize glucose-deficient mouse lungs (46, 55). It has been demonstrated that WT cryptococci harvested during pulmonary infection exhibit a gene expression profile consistent with a starvation response (47, 56, 57). Metabolic dysfunction due to the absence of IP_7, as suggested by our gene expression data, was supported by our observation of the severely reduced growth of the Δ*kcs1* mutant on alternative carbon sources, such as oleic acid, glycerol, and lactate (Fig. 9A). Utilization of these carbon sources requires functional mitochondria and, in the case of oleic acid, peroxisomes (58). A similar metabolic imbalance was reported for the Δ*kcs1* mutant of *S. cerevisiae* (59), whose cells did not grow on ethanol or glycerol as a sole carbon source.

Characterization of cryptococcal mutants defective in key metabolic enzymes established unequivocally the importance of β-oxidation and gluconeogenesis for the survival of *C. neoformans* in the nutrient-poor environment of the host and for pathogenicity. For example, a mutant in the peroxisomal β-oxidation pathway (Δ*mfe1* mutant) failed to grow on fatty acids as a carbon source and displayed hypovirulence in mice and reduced dissemination to the brain (49). Consistent with this report and with our observation that Δ*kcs1* mutant growth was reduced on oleic acid as the sole carbon source, *MFE1* expression in Δ*kcs1* cells was 21-fold lower than in WT cells (Table S3). Similarly, a gluconeogenesis-defective cryptococcal mutant deficient in phosphoenolpyruvate carboxykinase Pck1(Δ*pck1* mutant) failed to grow on lactate as a sole carbon source and was also markedly less virulent in mice (48). Figure 9B and Table S3 demonstrate that the expression of *PCK1* was lower in Δ*kcs1* cells than in the WT; the difference was 20-fold when the WT and Δ*kcs1* cells were grown in YPD and 2-fold when the strains were grown in minimal medium with lactate as a sole carbon source. Taken together, our findings suggest that the reduced pathogenicity of the Δ*kcs1* mutant may be due to a failure to adjust its metabolic response to a nutrient-poor environment, and this failure is caused, at least in part, by compromised regulation of gene expression. Such metabolic adaptation is essential for successful host infection.

Persistence of Δ*kcs1* mutant infection correlates with reduced surface mannoprotein. Despite the reduced pathogenicity and metabolic defects observed in the Δ*kcs1* mutant, a low level of apparently asymptomatic infection persisted *in vivo*. Our results suggest that this persistence of Δ*kcs1* mutant infection in lung is due primarily to the reduction in the display of surface mannoproteins in the Δ*kcs1* strain, as evidenced by decreased ConA binding and reduced expression of genes encoding immunogenic mannoproteins, leading to reduced recognition by phagocytes. It is likely that the majority of the opsonic anticryptococcal antibod-

ies in serum target mannoproteins (45, 60). Thus, the reduced mannoprotein content on the surfaces of Δ*kcs1* cells is expected to result in reduced opsonization by antibodies against mannoprotein and less efficient recognition of the fungal cells by phagocytic Fc receptors (45). Reduced phagocytosis of Δ*kcs1* cells indeed coincided with evidence of less phagocyte activation. The levels of phagocytosis of heat-killed WT and Δ*kcs1* cells were also compared to rule out the possibility that the reduction in phagocytosis of Δ*kcs1* cells by THP-1 monocytes was due to the lower proliferation rate of Δ*kcs1* cells. Again, the phagocytosis of killed Δ*kcs1* cells was reduced relative to that of WT cells (Fig. 8B). This reduction was even greater than that observed for live cells (~16-fold versus ~4-fold), possibly because a different concentration of serum was used for opsonization of the killed cells, as indicated in the legend of Fig. 8.

Persistent Δ*kcs1* strain lung infection may also be due to impaired sampling of mannoproteins by resident macrophages and dendritic cells for subsequent presentation to T cells, once again as a result of diminished mannoprotein production in Δ*kcs1* cells. Notably, the secreted polysaccharide deacetylase homolog Fpd1/D21 (CNAG_06291), which stimulates T-cell activation in mice and therefore contributes to the adaptive immune response to WT *C. neoformans* (61, 62), was down-regulated in Δ*kcs1* cells (Table 1). Transcription of many genes encoding proteases, including aspartic proteases (CNAG_06213, CNAG_04380, and CNAG_00581), carboxypeptidases (CNAG_01040 and CNAG_05973), serine-type endopeptidase (CNAG_04625), and elastinolytic metalloproteinase (CNAG_04735), was also reduced. Fungal proteases are known to elicit inflammatory responses via activation of protease-activated receptors (PARs), leading to allergic inflammation (63, 64). Thus, reduced secretion of proteases by the Δ*kcs1* mutant potentially contributes to the weak proinflammatory cytokine response and impaired infiltration of inflammatory neutrophils and monocytes observed in Δ*kcs1* mutant-infected lung (Fig. 7 and S4).

The persistence of Δ*kcs1* strain infection also correlated with a reduced recognition of Δ*kcs1* cells by the host immune system, as indicated by the lung cytokine profile (Fig. 7). First, in contrast to what occurred in WT-infected lung, no peak at day 7 was observed for the TNF, IFN-γ, and MCP-1 responses in Δ*kcs1* mutant-infected lung. This is consistent with a greater reduction in the proinflammatory response to Δ*kcs1* cells at day 7 when fungal burden is taken into account. Interestingly, however, similar IL-2 and IL-17A responses were obtained in WT- and Δ*kcs1*-infected lungs at day 14 despite the significantly lower Δ*kcs1* mutant burden. Taken together, the phagocytosis, lung cytokine, and histological data suggest that the persistence of a low-grade, asymptomatic Δ*kcs1* mutant infection is attributable to reduced recruitment of monocytes to sites of Δ*kcs1* mutant infection and reduced uptake of the Δ*kcs1* mutant by resident lung macrophages and infiltrating monocytes.

In summary, we have demonstrated for the first time that the IP biosynthetic pathway is essential for cryptococcal pathogenicity in a mammalian infection model. We have shown that Kcs1 is the major IP_6 kinase in *C. neoformans* producing IP_7, while Asp1 is an IP_7 kinase essential for the production of IP_8. We have established that, of the two PP-IPs, IP_7 exerts the greatest influence on cryptococcal pathogenicity. Our findings indicate that IP_7 affects cryptococcal cellular functions, at least in part, via gene expression and that successful host infection requires IP_7 to activate starvation-related metabolic pathways.

MATERIALS AND METHODS

Strains and media. Wild-type *C. neoformans* var. *grubii* strain H99 (serotype A, MAT**a**) was used in this study. The *ARG1* (CNAG_06500) deletion mutant (Δ*arg1* mutant) was described previously (24). The KN99 (MATα) strain was a kind gift from Joseph Heitman's laboratory (Duke University, Durham, NC, USA) (65). *C. neoformans* strains were maintained on SAB agar plates (4% dextrose, 1% peptone, 2% agar, pH 5.6), and incubated in YNB (6.7 g/liter yeast nitrogen base, 0.5% glucose), YPD (1% yeast extract, 2% peptone, and 2% dextrose), or MM (minimal medium; 15 mM glucose, 10 mM $MgSO_4$, 29.4 mM KH_2PO_4, 13 mM glycine, 3 μM thiamine) broth in preparation for the experiments. Mating was induced on 5% V8 juice (pH 5), 2% agar plates. MM without glucose was used for laccase induction in broth culture and for the preparation of broth and plates with different carbon sources (1% oleic acid, sodium lactate, or glycerol). Minimal medium plates supplemented with 1 mM L-DOPA (L-3,4-dihydroxyphenylalanine) were used to assess melanization.

Quantification of extracellular laccase activity. The protocol was adapted from reference 66. *C. neoformans* strains were grown overnight in YPD at 30°C. Cells were pelleted, washed with water, resuspended in MM without glucose at an optical density at 600 nm (OD_{600}) of 1, and incubated for 4 h at 30°C. To measure cell-associated laccase activity, 200 μl of the culture was removed and the cells were pelleted by centrifugation. The pellet was resuspended in 1 ml of a 3 mM concentration of a chromogenic laccase substrate, ABTS [2,2′-azinobis(3-ethylbenzothiazoline-6-sulfonic acid)], and incubated for 30 min at 30°C until a light blue color was produced, indicative of ABTS oxidation. The cells were pelleted, and the OD of the supernatant was measured at 436 nm. Laccase-specific activity was expressed as micromoles of ABTS substrate oxidized/minute/milliliter of culture at an OD_{600} of 1. The concentration of oxidized ABTS was calculated using the molar extinction coefficient ($\varepsilon = 29.3\ mM^{-1}\ cm^{-1}$).

[^{3}H]inositol labeling. [^{3}H]inositol labeling of cryptococcal cells was performed according to the protocol of reference 67, with several modifications. Briefly, fungal strains from overnight YPD culture were diluted in 5 ml fresh YPD to an OD_{600} of 0.01 (WT versus the Δ*kcs1* and Δ*arg1* mutants) or to an OD_{600} of 0.05 (WT versus the Δ*kcs1*::*KCS1*, Δ*kcs1*::*KCS1*^{AAA}, and Δ*asp1* strains), supplemented with 10 μCi/ml [^{3}H]myo-inositol (PerkinElmer), and incubated until the OD of the cultures reached at least 6 (16 to 76 h). The cells were pelleted, washed twice with 1 ml of fresh YPD, and snap-frozen in liquid nitrogen. To extract inositol polyphosphates, the cells were resuspended in extraction buffer (1 M $HClO_4$, 3 mM EDTA, 0.1 mg/ml IP_6) and homogenized in the presence of glass beads using a bead beater (four 30-s cycles with 1-min rests in between cycles). After the debris was pelleted, supernatants were neutralized using neutralization buffer (1 M K_2CO_3, 3 mM EDTA) and incubated on ice for 2 h. HPLC inositol phosphate analysis was performed as previously described (67).

Murine inhalation model of cryptococcosis. All procedures were approved by the Sydney West Local Health District Animal Ethics Committee, Department of Animal Care. Survival and organ burden/cytokine analyses were conducted using 7-week-old female BALB/c mice obtained from the Animal Resource Centre, Floreat Park, Western Australia. For both sets of analyses, mice were anesthetized using isoflurane (in oxygen) delivered via an isoflurane vaporizer attached to a Stinger small-animal anesthetic machine (Advanced Anaesthesia Specialists). Groups of 8 to 10 mice were then inoculated intranasally with the *C. neoformans* WT or IPK mutant strain (5×10^5 yeast cells in 20 μl phosphate-buffered saline [PBS]) and observed daily for signs of ill health. The number of viable yeast cells inoculated into the nares was later confirmed by quantitative culture.

For the survival study, mice which had lost 20% of their preinfection weight or which showed debilitating clinical signs prior to losing this

weight, including hunching, respiratory distress, excessive fur ruffling, or sluggish/unsteady movement, were euthanized by CO_2 inhalation followed by cervical dislocation. Δ*kcs1* mutant-infected mice were sacrificed 50 days postinoculation. Differences in survival were determined with SPSS version 21 statistical software, using the Kaplan-Meier method (log rank test), where a P value of <0.05 was considered statistically significant.

For calculating lung and brain infection burdens and determining lung cytokine profiles, 3 from a group of 9 mice infected with a particular strain (the WT or Δ*kcs1* mutant) were sacrificed 3, 7, and 14 days postinoculation. For lung cytokine analysis, 3 mock-infected mice sacrificed on days 3, 7, and 14, respectively, served as controls. For determining infection burdens, lungs and brains were harvested from infected mice, weighed, and homogenized in a total of 1 ml sterile PBS. One hundred microliters of each homogenate was removed and serially diluted 10-fold in sterile PBS, and 100 μl of each dilution was plated onto SAB agar. The plates were incubated for 2 to 3 days at 30°C, and the number of CFU was determined. The remainder of each lung homogenate (900 μl) and 900 μl of lung homogenate obtained from each of the control mice were centrifuged at 10,000 × *g* to pellet tissue debris, and the supernatants were collected and frozen for cytokine analysis.

Cytokine profiling in infected lung supernatant. Cytokine concentrations in lung homogenates collected postinfection were determined using mouse Th1/Th2/Th17 cytokine bead arrays (CBA; Becton, Dickinson Biosciences). MCP-1 was measured in a separate assay using the mouse MCP-1 flex set (bead B7) (BD Biosciences). CBA kits were used according to the manufacturer's instructions, data were collected using an LSRII flow cytometer, and results were analyzed using FCAP software version 3.0 (BD Biosciences).

Virulence in *Galleria mellonella*. *C. neoformans* WT and Δ*kcs1* mutant cells were grown overnight in YPD broth, pelleted by centrifugation, and resuspended in water at a concentration of 10^8 cells/ml. *G. mellonella* larvae (10 per strain) were inoculated with 10 μl of cell suspension (10^6 yeast cells) by injection into the hemocoel via the lower prolegs. The viability of each inoculum was assessed by performing serial 10-fold dilutions, plating the lowest dilutions on SAB agar plates, and counting the CFU after a 3-day incubation at 30°C. Inoculated larvae were monitored daily for 10 days after daily removal of their cocoon. Larvae were considered dead when they no longer responded to touch (68).

Phagocytosis experiments. THP-1 cells were maintained in RPMI 1640-10% fetal bovine serum (FBS) medium. IFN-γ (10 ng/ml) was added 24 h prior to the phagocytosis experiment to activate the monocytes. Cryptococcal cells were grown overnight in YNB broth, pelleted by centrifugation, and resuspended in staining solution (0.5 mg/ml FITC in PBS) for 30 min at 30°C. To heat kill fungal cells in some of the experiments, YNB cultures were centrifuged and the cell pellets were incubated at 56°C for 30 min prior to FITC staining. Following FITC staining, fungal cell pellets were washed three times with PBS and opsonized for 30 min at 30°C with human serum (10 to 100%, as indicated in the figures) or human IgG (Sigma-Aldrich I4506) or anti-GXM antibody 18B7 (a kind gift from Arturo Casadevall) in PBS (69). Opsonized fungal cells were pelleted and mixed with THP-1 monocytes in a ratio of 3:1 or 5:1 in THP-1 growth medium. Fungal and mammalian cells were coincubated for 3 to 5 h at 37°C in 5% CO_2. To quantify the adhesion/uptake of the fungal cells by THP-1, the cultures were mixed by pipetting, diluted with PBS, and analyzed by flow cytometry and microscopy. Reverse transcription-PCR (RT-PCR) was used to assess the THP-1 activation response to WT and Δ*kcs1* cells after 4 h of coincubation, using an RT^2 profiler PCR array designed for analysis of the antifungal immune response (SABiosciences). PCR was performed using a QuantStudio6 Flex real-time PCR system (Life Technologies). The expression data were normalized to the expression of the housekeeping GAPDH, ACTB, B2M, HPRT1, and RPLPO genes and then calculated as the fold change from expression in activated THP-1 cells that had not been coincubated with cryptococci.

Peripheral blood monocytes (PBMCs) were isolated from fresh human blood using a Ficoll-Paque gradient. Up to 20 ml of blood was layered on top of 15 ml of Ficoll-Paque and centrifuged at 400 × *g* for 30 min. The interphase containing monocytes and T and B lymphocytes was collected in a fresh tube and washed twice with PBS before resuspension of the final pellet in RPMI 1640-10% FBS medium. PBMCs were visualized with crystal violet stain and counted using a hemocytometer. PBMCs (4×10^6) were mixed with 4×10^6 heat-killed, FITC-labeled, 10%-serum-opsonized cryptococci in 100 μl of RPMI 1640-10% FBS medium and coincubated for 2 h at 37°C in 5% CO_2. The cell pellets were washed once with PBS. Nonspecific Fc receptor-mediated antibody binding was blocked before cells were stained with antigen-presenting cell (APC)-H7-conjugated anti-CD14 antibody (monocyte marker) (BD Biosciences; catalog number 560180). Adhesion/uptake of cryptococci by the CD14-positive cell population was quantified by flow cytometry and visualized by microscopy (70, 71; see Text S1 in the supplemental material).

Mannoprotein staining with ConA-FITC. Cryptococcal cells were grown overnight in YNB, washed with PBS, and resuspended in 100 μl PBS supplemented with 0.5% gelatin at an OD_{600} of 0.5. Each suspension was incubated for 30 min at room temperature. Ten microliters of ConA-FITC (Sigma; C7642) from a 2.5-mg/ml stock solution in water was added to each culture sample, followed by incubation for 30 min at room temperature. The extent of ConA-FITC binding was assessed using flow cytometry.

High-throughput gene expression analysis. Fungal strains were grown in YPD broth for 22 h. RNA was isolated using TRIzol and further purified using a Qiagen RNA isolation kit. Library preparation and sequencing were carried out by the Ramaciotti Centre for Genomics (UNSW, Sydney, Australia) using a TruSeq sample preparation kit and the Illumina HiSeq2000 sequencing platform to generate 100-bp paired-end reads. The resulting data were analyzed using the Galaxy platform (https://usegalaxy.org/). The analysis included data from three biological replicates for each strain; a ≥2-fold difference in gene expression between WT and Δ*kcs1* cells was considered to be significant. The presence of a signal peptide and N- and O-linked glycosylation were predicted using CBS prediction tools (http://www.cbs.dtu.dk/services/). The presence of a GPI anchor was predicted using the Big-PI fungal predictor (http://mendel.imp.ac.at/sat/gpi/fungi_server.html). Initial functional classification of cryptococcal genes was performed using GO term assignment from the Joint Genome Institute (JGI) database (http://genome.jgi.doe.gov/cgi-bin/ToGo?species=Cryne_ H99_1) and further improved based on the literature and by performing a homology search. A hypergeometric test was used to assess whether Kcs1-dependent genes were overrepresented in specific functional groups.

SUPPLEMENTAL MATERIAL

Supplemental material for this article may be found at http://mbio.asm.org/lookup/suppl/doi:10.1128/mBio.00531-15/-/DCSupplemental.

Text S1, DOCX file, 0.1 MB.
Figure S1, TIF file, 1 MB.
Figure S2, TIF file, 0.4 MB.
Figure S3, TIF file, 1.4 MB.
Figure S4, TIF file, 1.9 MB.
Figure S5, TIF file, 0.2 MB.
Figure S6, TIF file, 0.5 MB.
Table S1, DOC file, 0.1 MB.
Table S2, DOC file, 0.1 MB.
Table S3, PDF file, 0.1 MB.

ACKNOWLEDGMENTS

This work was supported by funding from a National Health and Medical Research Council of Australia project grant (APP1058779) and by Bioplatforms Australia through the Commonwealth Government National Collaborative Research Infrastructure Strategy (RNA-seq). A.S. is supported by the Medical Research Council (MRC core support to the MRC/UCL Laboratory for the Molecular Cell Biology University Unit [grant

MC_U122680443]), and T.C.S. is a Sydney Medical School Foundation Fellow.

We thank Ana Traven for helpful suggestions and Robert Lev for generous help with the RNA-seq data analysis. We also thank Virginia James and the Histology Department at WMIMR for performing mouse lung histology, Christabel F. Wilson for help with the animal infection studies, the WMI genomics facility for assistance with qPCR, the WMI flow cytometry and microscopy facilities for assistance with phagocytosis studies, and the sequencing team at the Ramaciotti Centre for Genomics (UNSW, Sydney, Australia).

REFERENCES

1. **Park BJ, Wannemuehler KA, Marston BJ, Govender N, Pappas PG, Chiller TM.** 2009. Estimation of the current global burden of cryptococcal meningitis among persons living with HIV/AIDS. AIDS **23:**525–530. http://dx.doi.org/10.1097/QAD.0b013e328322ffac.
2. **Hull CM, Heitman J.** 2002. Genetics of Cryptococcus neoformans. Annu Rev Genet **36:**557–615. http://dx.doi.org/10.1146/annurev.genet.36.052402.152652.
3. **Kozubowski L, Lee SC, Heitman J.** 2009. Signalling pathways in the pathogenesis of Cryptococcus. Cell Microbiol **11:**370–380. http://dx.doi.org/10.1111/j.1462-5822.2008.01273.x.
4. **Eisenman HC, Casadevall A.** 2012. Synthesis and assembly of fungal melanin. Appl Microbiol Biotechnol **93:**931–940. http://dx.doi.org/10.1007/s00253-011-3777-2.
5. **Perfect JR.** 2006. Cryptococcus neoformans: the yeast that likes it hot. FEMS Yeast Res **6:**463–468. http://dx.doi.org/10.1111/j.1567-1364.2006.00051.x.
6. **Doering TL.** 2009. How sweet it is! Cell wall biogenesis and polysaccharide capsule formation in Cryptococcus neoformans. Annu Rev Microbiol **63:**223–247. http://dx.doi.org/10.1146/annurev.micro.62.081307.162753.
7. **O'Meara TR, Alspaugh JA.** 2012. The Cryptococcus neoformans capsule: a sword and a shield. Clin Microbiol Rev **25:**387–408. http://dx.doi.org/10.1128/CMR.00001-12.
8. **Wang Y, Aisen P, Casadevall A.** 1995. Cryptococcus neoformans melanin and virulence: mechanism of action. Infect Immun **63:**3131–3136.
9. **Waterman SR, Hacham M, Panepinto J, Hu G, Shin S, Williamson PR.** 2007. Cell wall targeting of laccase of Cryptococcus neoformans during infection of mice. Infect Immun **75:**714–722. http://dx.doi.org/10.1128/IAI.01351-06.
10. **Bose I, Reese AJ, Ory JJ, Janbon G, Doering TL.** 2003. A yeast under cover: the capsule of Cryptococcus neoformans. Eukaryot Cell **2:**655–663. http://dx.doi.org/10.1128/EC.2.4.655-663.2003.
11. **Zaragoza O, Rodrigues ML, De Jesus M, Frases S, Dadachova E, Casadevall A.** 2009. The capsule of the fungal pathogen Cryptococcus neoformans. Adv Appl Microbiol **68:**133–216. http://dx.doi.org/10.1016/S0065-2164(09)01204-0.
12. **Kozel TR.** 1995. Virulence factors of Cryptococcus neoformans. Trends Microbiol **3:**295–299. http://dx.doi.org/10.1016/S0966-842X(00)88957-X.
13. **García-Rodas R, Zaragoza O.** 2012. Catch me if you can: phagocytosis and killing avoidance by Cryptococcus neoformans. FEMS Immunol Med Microbiol **64:**147–161. http://dx.doi.org/10.1111/j.1574-695X.2011.00871.x.
14. **Levitz SM, Specht CA.** 2006. The molecular basis for the immunogenicity of Cryptococcus neoformans mannoproteins. FEMS Yeast Res **6:**513–524. http://dx.doi.org/10.1111/j.1567-1364.2006.00071.x.
15. **Djordjevic JT, Del Poeta M, Sorrell TC, Turner KM, Wright LC.** 2005. Secretion of cryptococcal phospholipase B1 (PLB1) is regulated by a glycosylphosphatidylinositol (GPI) anchor. Biochem J **389:**803–812. http://dx.doi.org/10.1042/BJ20050063.
16. **Siafakas AR, Sorrell TC, Wright LC, Wilson C, Larsen M, Boadle R, Williamson PR, Djordjevic JT.** 2007. Cell wall-linked cryptococcal phospholipase B1 is a source of secreted enzyme and a determinant of cell wall integrity. J Biol Chem **282:**37508–37514. http://dx.doi.org/10.1074/jbc.M707913200.
17. **Eigenheer RA, Jin Lee Y, Blumwald E, Phinney BS, Gelli A.** 2007. Extracellular glycosylphosphatidylinositol-anchored mannoproteins and proteases of Cryptococcus neoformans. FEMS Yeast Res **7:**499–510. http://dx.doi.org/10.1111/j.1567-1364.2006.00198.x.
18. **Biondo C, Mancuso G, Midiri A, Bombaci M, Messina L, Beninati C, Teti G.** 2006. Identification of major proteins secreted by Cryptococcus neoformans. FEMS Yeast Res **6:**645–651. http://dx.doi.org/10.1111/j.1567-1364.2006.00043.x.
19. **Biondo C, Messina L, Bombaci M, Mancuso G, Midiri A, Beninati C, Cusumano V, Gerace E, Papasergi S, Teti G.** 2005. Characterization of two novel cryptococcal mannoproteins recognized by immune sera. Infect Immun **73:**7348–7355. http://dx.doi.org/10.1128/IAI.73.11.7348-7355.2005.
20. **Pietrella D, Cherniak R, Strappini C, Perito S, Mosci P, Bistoni F, Vecchiarelli A.** 2001. Role of mannoprotein in induction and regulation of immunity to Cryptococcus neoformans. Infect Immun **69:**2808–2814. http://dx.doi.org/10.1128/IAI.69.5.2808-2814.2001.
21. **Pietrella D, Corbucci C, Perito S, Bistoni G, Vecchiarelli A.** 2005. Mannoproteins from Cryptococcus neoformans promote dendritic cell maturation and activation. Infect Immun **73:**820–827. http://dx.doi.org/10.1128/IAI.73.2.820-827.2005.
22. **Huang C, Nong SH, Mansour MK, Specht CA, Levitz SM.** 2002. Purification and characterization of a second immunoreactive mannoprotein from Cryptococcus neoformans that stimulates T-cell responses. Infect Immun **70:**5485–5493. http://dx.doi.org/10.1128/IAI.70.10.5485-5493.2002.
23. **Chayakulkeeree M, Sorrell TC, Siafakas AR, Wilson CF, Pantarat N, Gerik KJ, Boadle R, Djordjevic JT.** 2008. Role and mechanism of phosphatidylinositol-specific phospholipase C in survival and virulence of Cryptococcus neoformans. Mol Microbiol **69:**809–826. http://dx.doi.org/10.1111/j.1365-2958.2008.06310.x.
24. **Lev S, Desmarini D, Li C, Chayakulkeeree M, Traven A, Sorrell TC, Djordjevic JT.** 2013. Phospholipase C of Cryptococcus neoformans regulates homeostasis and virulence by providing inositol trisphosphate as a substrate for Arg1 kinase. Infect Immun **81:**1245–1255. http://dx.doi.org/10.1128/IAI.01421-12.
25. **Luo HR, Huang YE, Chen JC, Saiardi A, Iijima M, Ye K, Huang Y, Nagata E, Devreotes P, Snyder SH.** 2003. Inositol pyrophosphates mediate chemotaxis in Dictyostelium via pleckstrin homology domain-PtdIns(3,4,5)P3 interactions. Cell **114:**559–572. http://dx.doi.org/10.1016/S0092-8674(03)00640-8.
26. **Saiardi A, Sciambi C, McCaffery JM, Wendland B, Snyder SH.** 2002. Inositol pyrophosphates regulate endocytic trafficking. Proc Natl Acad Sci U S A **99:**14206–14211. http://dx.doi.org/10.1073/pnas.212527899.
27. **York SJ, Armbruster BN, Greenwell P, Petes TD, York JD.** 2005. Inositol diphosphate signaling regulates telomere length. J Biol Chem **280:**4264–4269. http://dx.doi.org/10.1074/jbc.M412070200.
28. **Saiardi A, Resnick AC, Snowman AM, Wendland B, Snyder SH.** 2005. Inositol pyrophosphates regulate cell death and telomere length through phosphoinositide 3-kinase-related protein kinases. Proc Natl Acad Sci U S A **102:**1911–1914. http://dx.doi.org/10.1073/pnas.0409322102.
29. **Nagata E, Luo HR, Saiardi A, Bae BI, Suzuki N, Snyder SH.** 2005. Inositol hexakisphosphate kinase-2, a physiologic mediator of cell death. J Biol Chem **280:**1634–1640. http://dx.doi.org/10.1074/jbc.M409416200.
30. **Bhandari R, Juluri KR, Resnick AC, Snyder SH.** 2008. Gene deletion of inositol hexakisphosphate kinase 1 reveals inositol pyrophosphate regulation of insulin secretion, growth, and spermiogenesis. Proc Natl Acad Sci U S A **105:**2349–2353. http://dx.doi.org/10.1073/pnas.0712227105.
31. **Illies C, Gromada J, Fiume R, Leibiger B, Yu J, Juhl K, Yang SN, Barma DK, Falck JR, Saiardi A, Barker CJ, Berggren PO.** 2007. Requirement of inositol pyrophosphates for full exocytotic capacity in pancreatic beta cells. Science **318:**1299–1302. http://dx.doi.org/10.1126/science.1146824.
32. **Azevedo C, Burton A, Ruiz-Mateos E, Marsh M, Saiardi A.** 2009. Inositol pyrophosphate mediated pyrophosphorylation of AP3B1 regulates HIV-1 gag release. Proc Natl Acad Sci U S A **106:**21161–21166. http://dx.doi.org/10.1073/pnas.0909176106.
33. **Saiardi A, Caffrey JJ, Snyder SH, Shears SB.** 2000. The inositol hexakisphosphate kinase family. Catalytic flexibility and function in yeast vacuole biogenesis. J Biol Chem **275:**24686–24692. http://dx.doi.org/10.1074/jbc.M002750200.
34. **Dubois E, Scherens B, Vierendeels F, Ho MM, Messenguy F, Shears SB.** 2002. In Saccharomyces cerevisiae, the inositol polyphosphate kinase activity of Kcs1p is required for resistance to salt stress, cell wall integrity, and vacuolar morphogenesis. J Biol Chem **277:**23755–23763. http://dx.doi.org/10.1074/jbc.M202206200.
35. **Padmanabhan U, Dollins DE, Fridy PC, York JD, Downes CP.** 2009. Characterization of a selective inhibitor of inositol hexakisphosphate kinases: use in defining biological roles and metabolic relationships of

inositol pyrophosphates. J Biol Chem **284:**10571–10582. http://dx.doi.org/10.1074/jbc.M900752200.
36. **Pöhlmann J, Fleig U.** 2010. Asp1, a conserved 1/3 inositol polyphosphate kinase, regulates the dimorphic switch in Schizosaccharomyces pombe. Mol Cell Biol **30:**4535–4547. http://dx.doi.org/10.1128/MCB.00472-10.
37. **Feoktistova A, McCollum D, Ohi R, Gould KL.** 1999. Identification and characterization of Schizosaccharomyces pombe asp1(+), a gene that interacts with mutations in the Arp2/3 complex and actin. Genetics **152:** 895–908.
38. **Bhandari R, Saiardi A, Ahmadibeni Y, Snowman AM, Resnick AC, Kristiansen TZ, Molina H, Pandey A, Werner JK, Jr, Juluri KR, Xu Y, Prestwich GD, Parang K, Snyder SH.** 2007. Protein pyrophosphorylation by inositol pyrophosphates is a posttranslational event. Proc Natl Acad Sci U S A **104:**15305–15310. http://dx.doi.org/10.1073/pnas.0707338104.
39. **Saiardi A, Bhandari R, Resnick AC, Snowman AM, Snyder SH.** 2004. Phosphorylation of proteins by inositol pyrophosphates. Science **306:** 2101–2105. http://dx.doi.org/10.1126/science.1103344.
40. **Worley J, Luo X, Capaldi AP.** 2013. Inositol pyrophosphates regulate cell growth and the environmental stress response by activating the HDAC Rpd3L. Cell Rep **3:**1476–1482. http://dx.doi.org/10.1016/j.celrep.2013.03.043.
41. **Chakraborty A, Latapy C, Xu J, Snyder SH, Beaulieu JM.** 2014. Inositol hexakisphosphate kinase-1 regulates behavioral responses via GSK3 signaling pathways. Mol Psychiatry **19:**284–293. http://dx.doi.org/10.1038/mp.2013.21.
42. **Mulugu S, Bai W, Fridy PC, Bastidas RJ, Otto JC, Dollins DE, Haystead TA, Ribeiro AA, York JD.** 2007. A conserved family of enzymes that phosphorylate inositol hexakisphosphate. Science **316:**106–109. http://dx.doi.org/10.1126/science.1139099.
43. **Onnebo S, Saiardi A.** 2009. Inositol pyrophosphates modulate hydrogen peroxide signalling. Biochem J **423:**109–118. http://dx.doi.org/10.1042/BJ20090241.
44. **Herring AC, Lee J, McDonald RA, Toews GB, Huffnagle GB.** 2002. Induction of interleukin-12 and gamma interferon requires tumor necrosis factor alpha for protective T1-cell-mediated immunity to pulmonary Cryptococcus neoformans infection. Infect Immun **70:**2959–2964. http://dx.doi.org/10.1128/IAI.70.6.2959-2964.2002.
45. **Levitz SM.** 2010. Innate recognition of fungal cell walls. PLoS Pathog **6:**e1000758. http://dx.doi.org/10.1371/journal.ppat.1000758.
46. **Garnett JP, Baker EH, Baines DL.** 2012. Sweet talk: insights into the nature and importance of glucose transport in lung epithelium. Eur Respir J **40:**1269–1276. http://dx.doi.org/10.1183/09031936.00052612.
47. **Hu G, Cheng PY, Sham A, Perfect JR, Kronstad JW.** 2008. Metabolic adaptation in Cryptococcus neoformans during early murine pulmonary infection. Mol Microbiol **69:**1456–1475. http://dx.doi.org/10.1111/j.1365-2958.2008.06374.x.
48. **Panepinto J, Liu L, Ramos J, Zhu X, Valyi-Nagy T, Eksi S, Fu J, Jaffe HA, Wickes B, Williamson PR.** 2005. The DEAD-box RNA helicase Vad1 regulates multiple virulence-associated genes in Cryptococcus neoformans. J Clin Invest **115:**632–641. http://dx.doi.org/10.1172/JCI23048.
49. **Kretschmer M, Wang J, Kronstad JW.** 2012. Peroxisomal and mitochondrial beta-oxidation pathways influence the virulence of the pathogenic fungus Cryptococcus neoformans. Eukaryot Cell **11:**1042–1054. http://dx.doi.org/10.1128/EC.00128-12.
50. **Bosch D, Saiardi A.** 2012. Arginine transcriptional response does not require inositol phosphate synthesis. J Biol Chem **287:**38347–38355. http://dx.doi.org/10.1074/jbc.M112.384255.
51. **Resnick AC, Snowman AM, Kang BN, Hurt KJ, Snyder SH, Saiardi A.** 2005. Inositol polyphosphate multikinase is a nuclear PI3-kinase with transcriptional regulatory activity. Proc Natl Acad Sci U S A **102:** 12783–12788.
52. **Lipke PN, Kurjan J.** 1992. Sexual agglutination in budding yeasts: structure, function, and regulation of adhesion glycoproteins. Microbiol Rev **56:**180–194.
53. **Guerrero A, Jain N, Goldman DL, Fries BC.** 2006. Phenotypic switching in Cryptococcus neoformans. Microbiology **152:**3–9. http://dx.doi.org/10.1099/mic.0.28451-0.
54. **Jain N, Li L, Hsueh YP, Guerrero A, Heitman J, Goldman DL, Fries BC.** 2009. Loss of AllerGen 1 confers a hypervirulent phenotype that resembles mucoid switch variants of Cryptococcus neoformans. Infect Immun **77:** 128–140. http://dx.doi.org/10.1128/IAI.01079-08.
55. **Saumon G, Martet G, Loiseau P.** 1996. Glucose transport and equilibrium across alveolar-airway barrier of rat. Am J Physiol **270:**L183–L190.
56. **Fan W, Kraus PR, Boily MJ, Heitman J.** 2005. Cryptococcus neoformans gene expression during murine macrophage infection. Eukaryot Cell **4:**1420–1433. http://dx.doi.org/10.1128/EC.4.8.1420-1433.2005.
57. **Derengowski LDS, Paes HC, Albuquerque P, Tavares AH, Fernandes L, Silva-Pereira I, Casadevall A.** 2013. The transcriptional response of Cryptococcus neoformans to ingestion by Acanthamoeba castellanii and macrophages provides insights into the evolutionary adaptation to the mammalian host. Eukaryot Cell **12:**761–774. http://dx.doi.org/10.1128/EC.00073-13.
58. **Turcotte B, Liang XB, Robert F, Soontorngun N.** 2010. Transcriptional regulation of nonfermentable carbon utilization in budding yeast. FEMS Yeast Res **10:**2–13. http://dx.doi.org/10.1111/j.1567-1364.2009.00555.x.
59. **Szijgyarto Z, Garedew A, Azevedo C, Saiardi A.** 2011. Influence of inositol pyrophosphates on cellular energy dynamics. Science **334:** 802–805. http://dx.doi.org/10.1126/science.1211908.
60. **Zhang MX, Lupan DM, Kozel TR.** 1997. Mannan-specific immunoglobulin G antibodies in normal human serum mediate classical pathway initiation of C3 binding to Candida albicans. Infect Immun **65:**3822–3827.
61. **Biondo C, Beninati C, Delfino D, Oggioni M, Mancuso G, Midiri A, Bombaci M, Tomaselli G, Teti G.** 2002. Identification and cloning of a cryptococcal deacetylase that produces protective immune responses. Infect Immun **70:**2383–2391. http://dx.doi.org/10.1128/IAI.70.5.2383-2391.2002.
62. **Biondo C, Beninati C, Bombaci M, Messina L, Mancuso G, Midiri A, Galbo R, Teti G.** 2003. Induction of T helper type 1 responses by a polysaccharide deacetylase from Cryptococcus neoformans. Infect Immun **71:** 5412–5417. http://dx.doi.org/10.1128/IAI.71.9.5412-5417.2003.
63. **Boitano S, Flynn AN, Sherwood CL, Schulz SM, Hoffman J, Gruzinova I, Daines MO.** 2011. Alternaria alternata serine proteases induce lung inflammation and airway epithelial cell activation via PAR2. Am J Physiol Lung Cell Mol Physiol **300:**L605–L614. http://dx.doi.org/10.1152/ajplung.00359.2010.
64. **Yike I.** 2011. Fungal proteases and their pathophysiological effects. Mycopathologia **171:**299–323. http://dx.doi.org/10.1007/s11046-010-9386-2.
65. **Nielsen K, Cox GM, Wang P, Toffaletti DL, Perfect JR, Heitman J.** 2003. Sexual cycle of Cryptococcus neoformans var. grubii and virulence of congenic a and alpha isolates. Infect Immun **71:**4831–4841. http://dx.doi.org/10.1128/IAI.71.9.4831-4841.2003.
66. **Heung LJ, Luberto C, Plowden A, Hannun YA, Del Poeta M.** 2004. The sphingolipid pathway regulates Pkc1 through the formation of diacylglycerol in Cryptococcus neoformans. J Biol Chem **279:**21144–21153. http://dx.doi.org/10.1074/jbc.M312995200.
67. **Azevedo C, Saiardi A.** 2006. Extraction and analysis of soluble inositol polyphosphates from yeast. Nat Protoc **1:**2416–2422. http://dx.doi.org/10.1038/nprot.2006.337.
68. **Mylonakis E, Moreno R, El Khoury JB, Idnurm A, Heitman J, Calderwood SB, Ausubel FM, Diener A.** 2005. Galleria mellonella as a model system to study Cryptococcus neoformans pathogenesis. Infect Immun **73:**3842–3850. http://dx.doi.org/10.1128/IAI.73.7.3842-3850.2005.
69. **Casadevall A.** 1995. Antibody immunity and invasive fungal infections. Infect Immun **63:**4211–4218.
70. **Fraser JA, Subaran RL, Nichols CB, Heitman J.** 2003. Recapitulation of the sexual cycle of the primary fungal pathogen Cryptococcus neoformans var. gattii: implications for an outbreak on Vancouver Island, Canada. Eukaryot Cell **2:**1036–1045. http://dx.doi.org/10.1128/EC.2.5.1036-1045.2003.
71. **Toffaletti DL, Rude TH, Johnston SA, Durack DT, Perfect JR.** 1993. Gene transfer in Cryptococcus neoformans by use of biolistic delivery of DNA. J Bacteriol **175:**1405–1411.